NAVWEPS REPORT 8088
NOTS TP 3125
COPY 94

IMPACT AT INTERMEDIATE VELOCITIES INVOLVING CONTACT PHENOMENA

by

Werner Goldsmith

Research Department

ABSTRACT. Theoretical relations and experimental data are presented for the collision of two objects at intermediate velocities when both wave propagation and relative indentation of the bodies must be considered. Equations are developed that combine a description of wave phenomena in beams, bars, and plates with a law of contact. Experimental results are shown involving the impact of spheres and conically headed projectiles on bars and beams, and a comparison with the predictions of several theories is provided.

The analytical relations are based on equations of motion treating both bars and beams as one-dimensional systems, with the effect of second-order correction factors neglected. The theory of Hertz and a simple postulate concerning perfectly plastic flow at the contact point are compared with the results of tests designed to relate experimentally the contact force as a function of the indentation in a regime where the major portion of the cross section at the point of contact remains elastic. The data were obtained from strain-gage and framing camera measurements.

U.S. NAVAL ORDNANCE TEST STATION

China Lake, California

March 1963

U. S. NAVAL ORDNANCE TEST STATION

AN ACTIVITY OF THE BUREAU OF NAVAL WEAPONS

C. BLENMAN, JR., CAPT., USN
Commander

WM. B. McLEAN, PH.D.
Technical Director

FOREWORD

The author, Dr. Werner Goldsmith, is a consultant to the U. S. Naval Ordnance Test Station and Professor of Engineering Mechanics at the University of California, Berkeley.

This report is a summary of work on impact at intermediate velocities involving contact phenomena. The work was supported in part by the National Science Foundation and by Bureau of Naval Weapons Task Assignment RMMO-42-004/216-1/F008-08-006.

Released by
T. E. PHIPPS, Head,
Research Department
17 December 1962

Under authority of
WM. B. McLEAN
Technical Director

NOTS Technical Publication 3125
NAVWEPS Report 8088

Published by.....Research Department
Collation.....Cover, 31 leaves, abstract cards
First printing.....215 numbered copies
Security classification.....UNCLASSIFIED

1 Naval Ordnance Laboratory, White Oak (Guided Missile Warhead Section)
1 Naval Postgraduate School, Monterey
2 Naval Propellant Plant, Indian Head (Research and Development Department)
1 Naval Research Laboratory (Chemistry Division, Code 6130, R. R. Miller)
1 Naval Weapons Laboratory, Dahlgren (Technical Library)
2 Naval Weapons Services Office
1 Office of Naval Research Branch Office, Chicago
1 Office of Naval Research Branch Office, Pasadena
1 Operational Test and Evaluation Force
1 Bureau of Naval Weapons Representative, Azusa
2 Chief of Ordnance
    ORDTB (1)
    ORDTS (1)
2 Aberdeen Proving Ground
    Ballistic Research Laboratories (1)
    Development and Proof Services (1)
1 Army Research Office, Durham
1 Diamond Ordnance Fuze Laboratory (Library)
4 Frankford Arsenal
    Pitman-Dunn Laboratory (3)
    Library (1)
1 Ordnance Ammunition Command, Joliet (ORDLY-R-T)
1 Ordnance Test Activity, Yuma Test Station (A and A Division, S. Cohen)
3 Picatinny Arsenal (Library)
1 Radford Arsenal
1 Redstone Arsenal (Rocket Development Laboratory, Test and Evaluation Branch)
1 Rock Island Arsenal
3 White Sands Missile Range (ORDBS-Technical Library)
2 Headquarters, U. S. Air Force
    AFDRD-AN (1)
    AFDRD-CC (1)
1 Tactical Air Command, Langley Air Force Base (TPL-RQD-M)
1 Air Force Cambridge Research Laboratories, Laurence G. Hanscom Field
3 Air Proving Ground Center, Eglin Air Force Base
1 Air University Library, Maxwell Air Force Base
1 Holloman Air Force Base
1 AFSC Liaison Office, Aberdeen Proving Ground
10 Armed Services Technical Information Agency (TIPCR)
1 Defense Atomic Support Agency, Sandia Base
1 Weapons Systems Evaluation Group
1 Ames Research Center
1 Langley Research Center (Library)
1 Lewis Research Center
4 British Joint Services Mission, Ministry of Supply Staff (Reports Officer) via BuWeps (DSC)
4 Defence Research Member, Canadian Joint Staff (W) via BuWeps (DSC)
2 Aerojet-General Corporation, Azusa, Calif. (Librarian) via BuWepsRep
2 Allegany Ballistics Laboratory, Cumberland, Md.

NOMENCLATURE

a	Radius of crater at free surface
A	Area of cross section
b	Half thickness of plate or beam
c	Wave or phase velocity
c_1	Dilatational wave velocity
c_2	Shear wave velocity
c_g	Group velocity
c_o	Rod wave velocity, $c_o = \sqrt{E/\rho}$
c_R	Velocity of Rayleigh waves
E	Young's modulus
E_D	Dynamic Young's modulus
f	Coefficient of friction Wave number
F	Force
f,g	Functions
G	Lamé constant, $G = \frac{E}{2(1+\mu)}$
h'^2	$f^2 - p^2/c_1^2$
i	Index
k'^2	$f^2 - p^2/c_2^2$
k	Experimental constant in experimental indentation laws Polar radius of gyration

k_2	Constant in the Hertz theory of contact
l,m,n	Direction cosines
L	Bar length
L { }	Laplace operator
m	Mass
n	Exponent in experimental indentation laws
p	Circular frequency
p_o	Flow pressure
q_j	Component coordinate
r	Radial coordinate Radius
R	Bar radius
s	Position
t	Time
u_j	Component of displacement vector
v_o	Initial velocity
w	Transverse displacement
X	Eigenfunction
x,y,z	Rectangular coordinates
α	Approach
α_r	Permanent approach
β	Half-cone angle
β_1,β_2	Correction factors for one-dimensional longitudinal wave solution in bars
γ_{ij}	Component of shear strain
∇^2	Laplacian operator

Δ Dilatation

ϵ_i Component of normal strain

$\bar{\epsilon}_1, \bar{\epsilon}_2$ Warping parameters

η Ratio of average shear strain to shear strain at neutral axis

λ Lamé constant, $\lambda = \frac{\mu E}{(1+\mu)(1-2\mu)}$

Λ Wavelength

μ Poisson's ratio

ρ Mass density

ρ_t Target density

σ_i Normal stress component

σ_y Yield stress

τ Duration of contact
Variable of integration

τ_{ij} Shear stress component

ϕ Relaxation function

ϕ_i Frequency function, $\phi_i = \frac{\rho \omega_i^2 L^2}{\eta^2 i^2 \pi^2 G}$

ψ Creep function

ω Natural frequency, $\omega = \frac{p}{2\pi}$

IMPACT AT INTERMEDIATE VELOCITIES INVOLVING CONTACT PHENOMENA

The collision of two solids may involve a variety of processes whose existence and relative importance depend almost exclusively on the shapes and physical characteristics of the objects and, most important, on the relative impact velocity. The relevant mechanical behavior of the materials is ordinarily classified as being elastic, plastic, viscous, or a combination of these; a quantitative description of these properties is formulated as a relation between stresses and strains and, in the case of time-dependent effects, their respective rates. For example, glass is treated as an ideal elastic substance, while most metals are usually regarded as elastic up to a certain level, beyond which plastic deformation occurs. All synthetics and, under certain conditions, a few metals such as lead are considered to be either viscoelastic, viscoplastic, or elasto-viscous-plastic. For processes involving significant changes in temperature, the appropriate mechanical equation of state is coupled through this parameter to a second relation specifying the thermodynamic behavior of the material.

Impact is differentiated from static or rapid loading in that the forces acting at the contact point are created and removed in a very short time interval, generating stress waves that subsequently propagate throughout the entire system. In addition, the collision produces a relative indentation at the contact point except in the case of perfectly normal contact of plane-ended bars of identical cross section. It has been demonstrated by the drop of $\frac{1}{4}$-inch-diameter hardened steel ball bearings on extremely hard metallic plates (Ref. 1) that such an indentation results in a permanent crater except in the velocity region below about 3 in/sec, which is of insignificant practical importance. One further exception should be noted: The energy transmitted by wave action in the collision of spheres of equal size has been shown to be small compared to the initial kinetic energy of the system (Ref. 2), and is thus usually neglected relative to the energy consumed in the local indentation. In all other collisions involving neither compressibility effects nor disintegration of either striker or target, wave propagation and contact deformation constitute the predominant manifestations of the phenomenon. This regime involves stress levels roughly within two orders of magnitude of the yield stress and particle velocities below the velocity of sound in the material. In accordance with custom, the process is treated as isothermal for the sake of simplicity, so that temperature and other thermodynamic effects need not be considered.

At higher velocities, either or both of the impinging objects may fracture, shatter, or be pulverized with large attendant dissipation of energy. At still greater impact speeds, where pressures of the order of the elastic modulus of the substances are generated, the solids will no longer remain incompressible, and the event must be analyzed by the methods of hydrodynamics. Collisions in this domain are accompanied by shock heating and frequently by phase transitions or instantaneous vaporization of the participating bodies.

This presentation is concerned with the results of an experimental program that has been conducted to examine the effects of collisions of hard metallic strikers on metallic bars and beams. The materials and range of impact velocities were chosen so that a permanent indentation was generated at the contact point, but the propagation of plastic strain was limited to the vicinity of this region and did not permeate throughout the entire cross section. In consequence, the phenomena observed are governed by the elastic-wave effects in the target produced by the contact force which, in turn, depends upon the geometrical and kinematical conditions of the impact and the properties of the colliding materials. A major objective of the investigation was the establishment of force-indentation relations that govern the contact of strikers of various shapes with plane surfaces of various metals. To supply the proper background, a short summary of analyses of elastic-wave-propagation processes in simple structural members if first presented, followed by a brief description of various theoretical force-indentation relations derived on the basis of differing assumptions concerning the material behavior.

The process of wave propagation in solids without regard to its initiation has been studied extensively by analytical means; the results of these investigations have been summarized in a number of references (Ref. 3–13). The description of these phenomena invariably involves a combination of a differential equation of motion with a suitable equation of state; the solution of these relations, which expresses the effect of the transient, is profoundly affected by both the geometry and the assumed behavior of the medium. The largest amount of information has been developed for a homogeneous, isotropic, elastic material whose equation of state is represented by Hooke's law in the form

$$\sigma_j = \lambda\Delta + 2G\epsilon_j \qquad \tau_{jk} = G\gamma_{jk} \qquad j,k = 1,2,3 \tag{1}$$

where σ_j and τ_{jk} are the normal and shearing components of stress, ϵ_j and γ_{jk} the corresponding components of strain, the dilatation Δ is the sum of the normal strains, and λ and G are the elastic constants defining the medium, called the Lamé constants. The latter can be expressed in terms of the more familiar Young's modulus E and Poisson ratio μ by the relations

$$\lambda = \frac{\mu E}{(1+\mu)(1-2\mu)} \qquad G = \frac{E}{2(1+\mu)} \tag{2}$$

In conjunction with the usual definitions of infinitesimal strain and the fundamental law of Newtonian dynamics, Eq. 1 leads to the displacement equations of motion

$$G\nabla^2 u_j + (\lambda+G)\frac{\partial \Delta}{\partial q_j} = \rho \frac{\partial^2 u_j}{\partial t^2} \qquad j = 1,2,3 \tag{3}$$

where u_j are the components of the displacement vector, q_j are the corresponding coordinates, ∇^2 is the second Laplacian operator, and ρ is the mass density.

In a body of infinite extent, the solution of Eq. 3 is readily accomplished, as the requirements on stresses at bounding surfaces need not be considered. Since the displacement vector can be decomposed into an equivolumnial and an irrotational part, either component may be permitted to vanish separately, resulting in the differential equations

$$\ddot{u}_j = c_1^2 \nabla^2 u_j \qquad \ddot{u} = c_2^2 \nabla^2 u_j \qquad j = 1,2,3 \tag{4}$$

corresponding to dilatational and divergenceless waves, which travel with constant velocity of

$$c_1 = \sqrt{\frac{\lambda+2G}{\rho}} \qquad \text{and} \qquad c_2 = \sqrt{\frac{G}{\rho}} \tag{5}$$

respectively. The solution of Eq. 4 can be expressed either in the form

$$u_j = f(lx + my + nz - ct) + g(lx + my + nz + ct) \tag{6}$$

for a rectangular coordinate system, or as

$$u_j = \frac{1}{r}\left[f(r-ct) + g(r+ct)\right] \tag{7}$$

for a spherically symmetric case where u_j depends spatially only on radius r. Quantities l, m, and n denote direction cosines, and c is the appropriate wave velocity. It can also be shown (Ref. 14) that all plane waves in an infinite homogeneous isotropic elastic medium propagate with one of the two velocities given by Eq. 5.

The precise analysis of wave phenomena in elastic media with bounding surfaces is invariably accomplished by examination of the behavior of an infinite harmonic wave train of natural frequency $\omega = p/2\pi$ and wavelength $\Lambda = 2\pi/f$ exhibiting displacements

$$u_j = A_j e^{i(fq_j - pt)} \qquad j = 1,2,3 \tag{8}$$

The coefficient A_j, a function of the coordinates and the wavelength (or, alternatively, the frequency) describes the nature of the deformations, or mode shapes of the body and is determined by the type of wave assumed to be extant and the character of the boundary conditions. The latter also define a relation between p and f, known as the frequency equation, from which the velocity of propagation of a single wave component, known as the phase velocity $c = p/f$, is delineated. The rate of propagation of a number of components with nearly identical wavelengths is called the group velocity c_g, defined by

$$c_g = c - \Lambda \frac{dc}{d\Lambda} \tag{9}$$

and corresponds to the rate of energy transfer. If c is independent of wavelength, then $c = c_g$; the form of the wave is then transmitted throughout the body without change and the phenomenon is termed non-dispersive. In the reverse case, an alteration in the shape of a pulse consisting of various harmonic components will be produced by a dispersive mechanism that arises from successive reflections of waves between the bounding surfaces where additional pulses of similar and different mode shape are initiated. The pulse form and frequency spectrum for a given steady wave train can be used for an examination of the propagation of the corresponding transient upon superposition of components by means of a Fourier integral and subsequent synthesis of the pulse from the frequency diagram, a technique known as Kelvin's method of stationary phase (Ref. 15).

Exact solutions of the combination of Eq. 3 and 8 and the appropriate boundary conditions have been developed only for bodies infinite in the direction of propagation, particularly for the half-space, thin plates, straight circular bars, and shells. The first of these, initially described by Rayleigh (Ref. 16), leads to a surface wave exhibiting displacements u_x and u_y along axes in the free surface parallel and perpendicular to the direction of propagation and a displacement u_z along the normal to the free surface, respectively, given by

$$u_x = iBf\left[e^{-qz} - \frac{2qs}{s^2+f^2} e^{-sz}\right]e^{i(fx-pt)} \tag{10}$$

$$u_y = 0 \tag{11}$$

$$u_z = Bq\left[e^{-qz} - \frac{2f^2}{s^2+f^2} e^{-sz}\right]e^{i(fx-pt)} \tag{12}$$

where

$$s^2 = f^2\left[1 - \frac{c_R^2}{c_2^2}\right] \quad \text{and} \quad q^2 = f^2\left[1 - \frac{1-2\mu}{2-2\mu}\frac{c_R^2}{c_2^2}\right] \tag{13}$$

B is an arbitrary constant, and the wave exhibits a nondispersive phase velocity c_R determined by the frequency equation

$$\left(\frac{c_R}{c_2}\right)^6 - 8\left(\frac{c_R}{c_2}\right)^4 + \left(24 - 16\,\frac{1-2\mu}{2-2\mu}\right)\left(\frac{c_R}{c_2}\right)^2 + 16\left(\frac{1-2\mu}{2-2\mu} - 1\right) = 0 \qquad (14)$$

The character of such waves produced by various types of surface sources, known as Lamb's problem, has also been treated exhaustively. The second case, originally investigated by Rayleigh (Ref. 17) and Lamb (Ref. 18), led to the frequency equations

$$\frac{\tanh k'b}{\tanh h'b} = \frac{4f^2h'k'}{(f^2+k'^2)^2} \qquad \text{and} \qquad \frac{\tanh k'b}{\tanh h'b} = \frac{(f^2+k'^2)^2}{4f^2h'k'} \qquad (15)$$

where

$$h'^2 = f^2 - \frac{p^2}{c_1^2} \qquad \text{and} \qquad k'^2 = f^2 - \frac{p^2}{c_2^2} \qquad (16)$$

for the symmetric and antisymmetric modes of each motion, respectively, and where b denotes the half-thickness of the plate. Equation 15 exhibits an infinite number of roots, each corresponding to a harmonic of the appropriate mode of transmission. A number of additional results for this situation have recently been described, encompassing symmetric, antisymmetric, and torsional motions and their coupled effects.

The circular bar, initially treated by Pochhammer (Ref. 19) and Chree (Ref. 20), has also been found to permit three basic modes of transmission, each of which exhibits an infinite number of harmonics, corresponding to symmetric (longitudinal), antisymmetric (bending), and shear waves, respectively (Ref. 4 and 14). The complicated frequency equations for the first two types of modes have been solved numerically, and the results for the first three harmonics are shown in Fig. 1 and 2 for a value of $\mu = 0.29$, corresponding to steel (Ref. 6 and 21). The lowest harmonic of the torsional mode is nondispersive and propagates with velocity c_2. A generalization of the analysis for the circular rod has recently been published that includes coupling between the modes and also gives an excellent account of approximate theories (Ref. 22). Corresponding results have been established for shells (Ref. 23–30), while other studies have been conducted to expose the complex branches of the frequency spectrum that delineate nonpropagating waves (Ref. 31 and 32). The analytical developments have often been supported by experimental investigations (Ref. 33–36).

The rigorous solutions of elastodynamics cannot be readily applied to a study of impact problems due to both their complicated form and their failure to encompass bodies of finite dimensions in the direction of propagation. The second difficulty arises from the fact that the stress-free conditions on the terminal faces have thus far prevented the establishment of an exact three-dimensional analysis. Accordingly,

various approximations have been devised that incorporate a considerably lower level of mathematical complexity and correspondingly greater manageability and permit a description of wave processes in finite bodies, yet still retain the essential physical features of the "exact" equations. The simplifications involved most frequently assume the form of solely one-dimensional considerations and the hypothesis of plane cross sections remaining plane. The efficacy of such approximate theories is usually judged by the degree of correlation between their phase and group velocity spectra and those of the rigorous solutions.

One-dimensional representations have been developed for rods, beams, plates, curved bars, and other simple structures for a variety of boundary conditions. Under the assumption of uniform stress distribution across any section and the neglect of radial inertia, the equation for longitudinal wave propagation in the bar is given by

$$\ddot{u} = c_o^2 \frac{\partial^2 u}{\partial x^2} \qquad \text{where} \qquad c_o = \sqrt{\frac{E}{\rho}} \tag{17}$$

in terms of displacement u in the x-direction. The solution of this equation is given by

$$u = f(x - c_o t) + g(x + c_o t) \tag{18}$$

that indicates a nondispersive phenomenon propagating at constant "rod" velocity c_o. Inspection of Fig. 1 reveals that this behavior corresponds to the lowest harmonic of the exact solution only for wavelengths large (greater than 5) relative to the characteristic dimension, or equivalent radius, of the bar. Functions f and g, related by the boundary condition at the distal end of the bar, are uniquely determined by the initial shape of the pulse. In consequence, the displacement u(x,t) resulting from the action of a time-dependent force applied over the terminal face x = 0 of a bar of length L can be expressed as

$$\begin{aligned} u(x,t) &= 0 && t < \frac{x}{c_o} \\ u(x,t) &= \frac{1}{\rho A c_o} \int_o^t F(t - \frac{x}{c_o})dt && t \geq \frac{x}{c_o} \end{aligned} \tag{19}$$

during the initial passage of the pulse. Additional terms must be introduced on the right-hand side of this equation whenever the effect of subsequent reflections at either end of the bar is first experienced at position x.

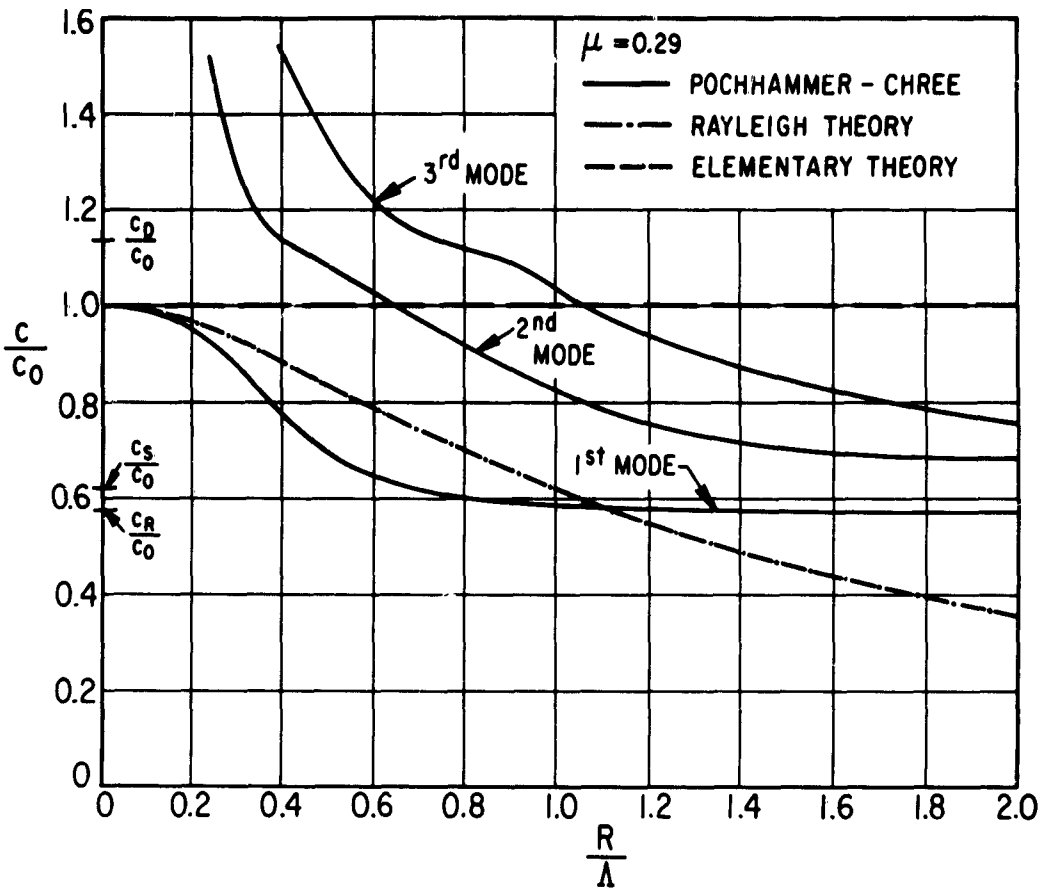

FIG. 1. Phase Velocity of Longitudinal Waves in Cylindrical Rods of Infinite Length.

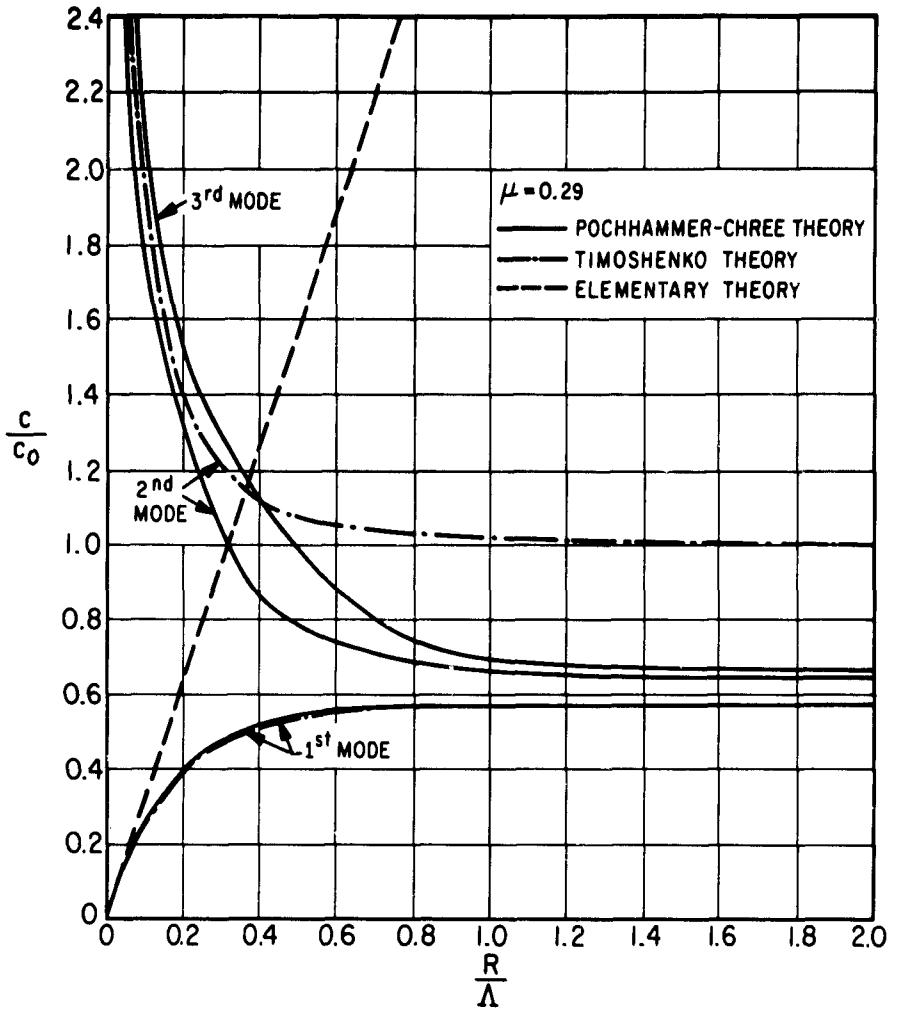

FIG. 2. Phase Velocity of Transverse Waves in Cylindrical Rods of Infinite Length.

The next higher approximation incorporates the effect of radial inertia in the wave equation, which is now given by (Ref. 14)

$$\ddot{u} - \mu^2 k^2 \frac{\partial^4 u}{\partial x^2 \partial t^2} = c_o^2 \frac{\partial^2 u}{\partial x^2} \quad \text{where} \quad c = \frac{p}{f} = \frac{c_o}{\sqrt{1 + \mu^2 k^2 f^2}} \tag{20}$$

where k is the polar radius of gyration of the section. This model yields a better correlation over a wider range of wavelengths for the phase velocity of the lowest harmonic with the exact solution, as shown in Fig. 1, but leads to the incorrect limit $c \to 0$ as Λ approaches 0 (thus permitting an infinite velocity of propagation of the wave front) (Ref. 15), for which the actual value should be $c \to c_2$. The wave phenomenon described by Eq. 20 is dispersive, and the displacement resulting from a force F(t) suddenly applied at the origin x = 0 of a semi-infinite rod at time t = 0 is

$$u(x,t) = 0 \qquad t < \frac{x}{c_o}$$

$$u(x,t) = \frac{1}{\rho A c_o} \int_o^t \frac{e^{\frac{-\tau x}{c_o \sqrt{1 + \frac{\mu^2 k^2}{c_o^2} \tau^2}}}}{\tau \sqrt{1 + \frac{\mu^2 k^2}{c_o^2} \tau^2}} F(t-\tau) d\tau \qquad t \geq \frac{x}{c_o} \tag{21}$$

that may be compared with Eq. 19.

An additional refinement accounts for the action of radial shear stresses that may be introduced by one of several techniques. The first of these (Ref. 37) involves the integration of the transverse stresses over the cross section, which leads to an improved expression for the axial stress in terms of displacement u. Upon substitution in the one-dimensional equation of motion, there results the relation

$$\ddot{u} = c_o^2 \frac{\partial^2 u}{\partial x^2} + \mu^2 k^2 \frac{\partial^4 u}{\partial x^2 \partial t^2} - \mu^2 k^2 c_2^2 \frac{\partial^4 u}{\partial x^4} \tag{22}$$

that exhibits a phase velocity given by

$$c = c_o \left(\sqrt{1 + \frac{\mu^2 k^2 f^2}{c_o^2}} \right) / \sqrt{1 + k^2 \mu^2 f^2} \tag{23}$$

The second method (Ref. 38-40) defines two relations for the axial and shear stresses, respectively, in terms of axial and radial displacements

u_z and u_r that contain two arbitrary correction factors β_1 and β_2 for a circular bar of radius R, which lead to the differential equations

$$\beta_1^2 R^2 G \frac{\partial^2 u_z}{\partial x^2} - 8\beta_2^2(\lambda+G)u_z - 4\beta_1\lambda R \frac{\partial u_r}{\partial z} = \rho R^2 \ddot{u}_z$$

$$2\beta_1\lambda R \frac{\partial u_z}{\partial z} + (\lambda+2G)R^2 \frac{\partial^2 u_r}{\partial z^2} = \rho R^2 \ddot{u}_r \tag{24}$$

and a phase velocity relation

$$\left[\beta_1^2 c_2^2 - \frac{8\beta_2^2}{k^2R^2}(c_1^2-c_2^2)-c^2\right]\left[c_1^2-c^2\right] - \frac{8\beta_2^2}{k^2R^2}(c_1-2c_2^2)^2 = 0 \tag{25}$$

Factors β_1 and β_2 are adjusted so as to provide an optimum fit of Eq. 25 with the lowest harmonic of the exact relation as shown in Fig. 1. Reference 41 presents a critical discussion of the efficacy of these two methods, while alternative procedures (Ref. 42–44) summarized in Ref. 22, do not afford any improvement in these results relative to the predictions of the Pochhammer-Chree equations. For any of these theories, however, the displacements produced by time-dependent forces can only be computed approximately under limiting conditions and even then only with enormous effort.

The zero-order approximation for the transverse or bending motion of a uniform beam of cross sectional area A and length L is known as the Euler equation. In terms of displacement w, it is given by

$$c_o^2 k_1^2 \frac{\partial^4 w}{\partial x^4} + \ddot{w} = 0 \tag{26}$$

that leads to a phase velocity

$$c = c_o f k_1 \tag{27}$$

where k_1 is the radius of gyration of the section about a centroidal axis perpendicular to the plane of bending. Displacements resulting from the action of a force F(s,t) applied at position x = s can be determined from the relation

$$w = \frac{1}{\rho A} \sum_{i=1}^{\infty} \frac{[X_i(s)]^2}{\omega_i \int_o^L X_i^2 dx} \int_o^t F(\tau)\sin\omega_i(t-\tau)d\tau \tag{28}$$

where eigenfunctions X_i and frequencies ω_i can be derived from Eq. 26 for any set of boundary conditions. For a simply supported beam, where $X_i = \sin i\pi x/L$ and $\omega_i = i^2\pi^2 c_o k_1/L^2$, the deflection due to a central load $F(\frac{1}{2}L,t)$ is given by

$$w(x,t) = \frac{2L}{\pi^2 c_o k_1 \rho A} \sum_{i=1,3,5\ldots}^{\infty} \frac{(-1)^{\frac{i-1}{2}} \sin \frac{i\pi x}{L}}{i^2} \int_o^t F(\tau)\sin \omega_i(t-\tau)d\tau \qquad (29)$$

Examination of Eq. 27 and Fig. 2 indicates that reasonable correspondence of the phase velocity with the first harmonic of the Pochhammer-Chree relations prevails only at very long wavelengths and that infinitely short wavelength components propagate at infinite velocities. This obvious physical defect has resulted in the addition of various correction terms, including some or all of the effects of rotatory inertia, transverse shear, warping of the section, and lateral contraction (Ref. 42-46). The most widely employed of these is the Timoshenko equation (Ref. 47), which incorporates the first two of these features and is given by

$$c_o^2 k_1^2 \frac{\partial^4 w}{\partial x^4} - k_1^2\left[1 + \frac{E}{\eta G}\right]\frac{\partial^4 w}{\partial x^2 \partial t^2} + \frac{\rho k_1^2}{\eta G}\frac{\partial^4 w}{\partial t^4} + \frac{\partial^2 w}{\partial t^2} = 0 \qquad (30)$$

The phase velocity for this equation can be determined from the relation

$$\left(\frac{c_o}{c}\right)^2 + \frac{E}{\eta G}\left(\frac{c}{c_o}\right)^2 = 1 + \frac{1}{f^2 k_1^2} + \frac{E}{\eta G} \qquad (31)$$

that admits of two sets of roots corresponding to the two lowest harmonics of the Pochhammer solution, the result being shown in Fig. 2. Term η represents the ratio of average shear strain across the section to that at the neutral axis; values of 0.667 and 0.75 have been computed for a rectangular and circular cross section, respectively, under the assumption of the existence of a distribution identical to that occurring during static loading. Alternatively, values of 0.822 and 0.847 have been proposed for the same section geometries so that an optimum fit between the spectrum of Eq. 31 and that of the exact equations is obtained.

When warping of the cross section is also considered, Eq. 30 and 31 are slightly modified, yielding

$$c_o^2 k_1^2 \frac{\partial^4 w}{\partial x^4} - k_1^2\left[1 + \frac{\bar{\epsilon}_1 E}{\eta G}\right]\frac{\partial^4 w}{\partial x^2 \partial t^2} + \rho\frac{\bar{\epsilon}_1 k_1^2}{\eta G}\frac{\partial^4 w}{\partial t^4} + \frac{\partial^2 w}{\partial t^2} = 0 \qquad (32)$$

$$\left(\frac{c_o}{c}\right)^2 + \frac{\bar{\epsilon}_1 E}{\eta G}\left(\frac{c}{c_o}\right)^2 = 1 + \frac{1}{f^2 k_1^2} + \frac{\bar{\epsilon}_1 E}{\eta G} \tag{33}$$

The deflection of a simply supported beam under the action of a central load is now given by (Ref. 13)

$$w(x,t) = \sum_{i=1,3,5\ldots}^{\infty} \frac{(-1)^{\frac{i-1}{2}}}{B_i \omega_i} \sin\frac{i\pi x}{L} \int_o^t F(\tau)\sin\omega_i(t-\tau)d\tau \tag{34}$$

where

$$B_i = \tfrac{1}{2}\rho AL\left[1 + \frac{i^2\pi^2 k_1^2}{L^2}(1 - 2\bar{\epsilon}_1\phi_i + \bar{\epsilon}_2\phi_i^2)\right] \qquad \phi_i = \frac{\rho\omega_i^2 L^2}{\eta^2 G i^2 \pi^2} \tag{35}$$

and freqency ω_i is determined from

$$\omega_i^2 = \left\{1+k_1^2\left(1 + \frac{\bar{\epsilon}_1 E i^2\pi^2}{\eta G L^2}\right) \pm \sqrt{\left[1+k_1^2\left(1+\frac{\bar{\epsilon}_1 E}{\eta G}\right)\frac{i^2\pi^2}{L^2}\right]^2 - \frac{4Ek_1^4 i^4\pi^4\bar{\epsilon}_1}{\eta G L^4}}\right\} \Big/ \left(\frac{2\rho\bar{\epsilon}_1 k_1^2}{\eta G}\right) \tag{36}$$

Eq. 34 must be summed over the two sets of frequencies derived from Eq. 33. Warping parameters $\bar{\epsilon}_1$ and $\bar{\epsilon}_2$ in Eq. 32, 33, and 35 can again be computed by considering the dynamic strain distribution to be the same as that under static conditions, yielding values of $\bar{\epsilon}_1 = 0.800$, $\bar{\epsilon}_2 = 68/105$ for a rectangular and $\bar{\epsilon}_1 = 5/6$, $\bar{\epsilon}_2 = 101/144$ for a circular cross section, respectively. Corrections incorporated in the one-dimensional theory of torsional wave propagation in a circular rod (Ref. 22) still yield the same nondispersive wave velocity c_2 derived for the lowest harmonic of the corresponding exact solution.

Although not of immediate concern in this presentation, departure of a material from homogeneous isotropic elasticity introduces serious complications in the corresponding analysis of wave-propagation processes, since a considerably more sophisticated constitutive equation must now be introduced into the equations of motion. Such substances are classified according to the character of the relation describing the general mechanism of deformation and may be categorized under the following headings: aeolotropic elastic, multiple phase and granular, elastoplastic, and viscoelastic. In spite of the early stipulation of the general stress-strain relations for the first of these classes (Ref. 14), the development of wave-propagation theories in such materials is still in an embryonic state even for bodies of infinite extent, and virtually nonexistent for bounded configurations (Ref. 7). The establishment of suitable constitutive equations and the development of wave analyses for

substances in the second group has received increasing attention in recent years (Ref. 48–51), but theoretical predictions based on the simple models postulated are not as yet adequately corroborated by experimental results.

During the last two decades, investigations concerning wave processes in elasto-plastic materials have been pursued energetically; in addition to bodies without bounds, the dynamic deformation of rods, wires, beams, slabs, plates, membranes, and shells have been mathematically described and, in some cases, experimentally ascertained. Two separate approaches for the specification of the equation of state have been adopted: In the first, the stress is considered to be a function solely of the state of strain, while the second also incorporates a dependence upon the rate of load application. The first procedure leads to a much simpler mathematical formulation of the problem, but appears to be applicable only to those materials not exhibiting a yield point and little strain-rate sensitivity, such as single crystals of aluminum. Considerable controversy prevails at the present time concerning both the applicability and physical significance of either of these hypotheses, particularly when these formulations are related to the predictions of the theory of dislocations. Furthermore, experimental verification of either of these postulates has been frequently obscured by inability to isolate the rate effects from other disturbing influences produced either by the manner of loading or geometrical constraints. A summary of advances in this area may be found in Ref. 9, 12, and 13.

Wave-propagation analyses in viscoelastic bodies have been confined almost entirely to linear materials, that is, those in which the superposition of a set of stress pulses produces a strain history equal to the sum of the strain cycles generated by each pulse. Many synthetic materials, including some of the more common photoelastic substances, conform to this requirement and exhibit significant anelastic effects in the linear range. Most metals, however, are not encompassed by such a description, remaining essentially elastic until a permanent set not explicitly dependent on time is initiated. Viscoelastic materials, which include the well-known Kelvin-Voigt, Maxwell, and standard linear solid, are described in terms of two functions ψ and ϕ that are simply related in terms of their Laplace transforms. The creep function ψ defines the strain history under the action of an applied stress, while the relaxation function ϕ denotes the stress response due to the application of a time-dependent strain. Under uniaxial conditions, this is described by

Applied load	Response	
$\sigma_x = 0$	$\epsilon_x(t) = 0$	$t < 0$
Creep:		(37)
$\sigma_x = \sigma_x(t)$	$\epsilon_x(t) = \frac{1}{E_D}\left\{\sigma_x(t) + \int_{-\infty}^{t} \frac{d\sigma_x(\tau)}{d\tau}\, \psi_x(t-\tau)\, d\tau\right\}$	$t \geq 0$

$$\epsilon_x = 0 \qquad \sigma_x(t) = 0 \qquad t < 0$$

Relaxation: (38)

$$\epsilon_x = \epsilon_x(t) \quad \sigma_x(t) = E_D \left\{ \epsilon_x(t) - \int_{-\infty}^{t} \frac{d\epsilon_x(\tau)}{d\tau} \phi_x(t-\tau) d\tau \right\} \qquad t \geq 0$$

where E_D is the dynamic Young's modulus. Dynamic problems involving these materials have been most frequently analyzed by operational methods; when the boundary conditions are invariant in time, a correspondence principle exists for these substances. In accordance with this principle, the governing equation of the system can be determined in the transformed plane from the identical elastic case upon replacement of the shear modulus G by the term $G(1 - L\{\psi_x\})$ where $L\{\ \}$ denotes the Laplacian operator.

Solutions of viscoelastic wave-propagation problems have been virtually limited to one-dimensional motion (Ref. 9, 13, and 52–57) and generally require either a number of approximations or numerical integration or both. However, the results obtained provide some measure of the attenuation of the pulse and the dispersion produced by the viscous effects. Variations of phase velocity and attenuation with frequency have also been determined experimentally (Ref. 10, 58, and 59). A general account of this topic is given in Ref. 60.

A number of equations have been proposed that express the force of contact F for two bodies subjected to mutual compression along the common normal to their surfaces at the contact point in terms of the total deformation along this line, a quantity called the approach α. The classical relation of this type was derived by Hertz (Ref. 61) on the basis of an electrostatic analogy for the static compression of two elastic bodies whose contact surfaces could be described by equations of the second degree. This equation states that

$$F = k_2 \alpha^{3/2} \tag{39}$$

where k_2 is a constant dependent upon the geometrical and elastic properties of the bodies. The value of k_2 is given by

$$k_2 = \frac{4}{3} \sqrt{R} \left[\frac{1-\mu_1^2}{E_1} + \frac{1-\mu_2^2}{E_2} \right]^{-1} \tag{40}$$

for the indentation of a plane surface "1" by a body "2" with a spherical contact surface of radius R. Equation 39 is inapplicable when the indenter is either conical, pyramidal, or wedge-shaped, since the geometrical restriction imposed on the use of this relation is violated. The Hertz law has been remarkably successful in predicting many experimentally observed features of indentation processes not only under static,

but also under dynamic conditions where plastic flow did not permeate throughout the entire cross section. The explanation for this correlation can be found in the fact that only a small percentage of the initial impact energy was employed to produce the plastic dent. The applicability of the relation, under these circumstances, is, however, questionable on theoretical grounds since its derivation is based on successive equilibrium states, and the permanent crater produced except at minimal velocities is not encompassed by this law. The Hertz relation has been extended to the contact of viscoelastic bodies (Ref. 62-64), but its validity is restricted to the approach phase of the process.

The variation of the contact force for the quasi-static indentation of a sphere of radius R with the radius of the permanent crater a was determined empirically by Meyer (Ref. 65 and 66) from a large number of tests in the plastic range as

$$F = Ca^2(a/R)^{n-2} \tag{41}$$

where C and n are constants for a particular set of materials. For a given size of the indenter, Eq. 41 may be expressed as

$$F = ka^n \qquad \text{where} \qquad k = \frac{C}{R^{n-2}} \tag{42}$$

that bears a superficial resemblance to the form of Eq. 39. The value of n for most work-hardened metals was found to be slightly larger than 2 and that for fully annealed metals was observed to be about 2.5 for crater sizes greater than 0.1 (Ref. 66). It has been suggested that the Meyer relation could be extended to include collisions in a manner similar to the extrapolation of the applicability of the Hertz equation for the corresponding elastic case (Ref. 67 and 68).

A widely employed device leading to considerable mathematical simplification of the analysis of indentation processes has been the stipulation of a constant average resistive pressure or mean flow pressure p_o at the interface. The use of such a postulate for the contact of a completely rigid sphere and a deformable semi-infinite solid reduces Eq. 42 to

$$F = \pi p_o(2R\alpha - \alpha^2) \tag{43}$$

or

$$F \approx 2\pi p_o R\alpha \tag{44}$$

provided α is not too large. Actually, a theoretical solution for the limiting condition of incipient plastic flow based on the stress distribution resulting from the use of Eq. 39 predicts that the magnitude of p_o at this stage is given by $p_o \approx 1.1\ \sigma_y$, where σ_y is the uniaxial yield stress (Ref. 1). On the other hand, both theoretical and experimental evidence indicates that, under quasi-static conditions of fully plastic flow, the magnitude of $p_o \approx 3\sigma_y$ or possibly even higher in the presence of significant frictional effects (Ref. 66). The assumption of a

constant flow pressure is thus a priori an approximation that is at best only roughly satisfied during certain phases of the indentation process. Other quasi-theoretical relations for the value of the flow pressure generated during the impact of a sphere on a half-space have been proposed as a function of the initial energy, the volume of the indentation, the coefficient of restitution, and the Meyer index n of Eq. 42 (Ref. 66).

A combination of Eq. 39 and the constant flow pressure hypothesis was employed to construct a theory for the collision of soft metallic spheres (Ref. 69 and 70). This analysis encompasses three regimes: (1) an initial elastic compression governed by Eq. 39; (2) an additional plastic deformation in a central region occurring at constant pressure p_o, surrounded by an elastic annulus; and (3) a restitution process involving elastic recovery of the plastic zone. Although subject to valid criticism, this theory has achieved a modicum of success in predicting contact durations and terminal velocities of the colliding spheres at impact velocities below 25 in/sec. Equation 44 has also been employed in the correlation of experimental data in the same velocity range for the impact of crossed cylinders whose elastic restitution process was considered to be governed by Eq. 39 with α replaced by $\alpha - \alpha_r$, where α_r is the terminal approach under no load, or permanent crater depth (Ref. 71).

An elastic regime is not present in the case of the penetration of a plane surface by a hard conical or pyramidal indenter, as plastic flow is generated instantaneously. A number of penetration relations have been proposed for the conical indenter of mass m on the basis of a constant flow pressure assumption and negligible restitution (Ref. 66 and 72), the simplest being

$$F = \pi p_o \alpha^2 \tan^2\beta = \pi p_o a^2 \tag{45}$$

where β is the half-cone angle and $p_o = 3\sigma_y$. When frictional effects in the form of a constant coefficient f and inertial effects of the target due to a term $\rho_t \dot{\alpha}^2$ are also considered, Eq. 45 is modified to read (Ref. 73)

$$F = \frac{\pi \tan\beta(\sin\beta + f\cos\beta)}{\cos\beta} \alpha^2 \left[p_o + \rho_t v_o^2 \sin^2\beta\right] e^{\frac{-2\pi\rho_t}{3m}(\sin\beta + f\cos\beta)\alpha^3 \tan^2\beta \sin\beta} \tag{46}$$

where ρ_t is the density of the target and v_o the initial velocity. When the quantity $\rho_t \dot{\alpha}^2$ is small compared to p_o, Eq. 46 reduces to

$$F = \frac{\pi \tan\beta(\sin\beta + f\cos\beta)}{\cos\beta} p_o \alpha^2 \tag{47}$$

Both Eq. 45 and 47 represent special cases of Eq. 42 with n = 2.

Since only meager experimental evidence exists concerning the accuracy of the postulated force-indentation relations at low impact velocities and is not available at intermediate velocities, a comprehensive program of tests has been undertaken to check the validity of such proposed equations under dynamic conditions over a wide spectrum of initial velocities for strikers with spherical and conical contact surfaces (Ref. 74–76). A comparison of the results with data obtained for similar geometries under quasi-static conditions was also performed to determine whether the latter could serve as an acceptable substitute for the corresponding dynamic relation or else could be so converted by means of a simple correction factor. Such a procedure would be of considerable practical value since experimental investigations of this type are far more easily and accurately performed under quasi-static loading conditions. Establishment of suitable dynamic force-indentation equations permits, at least in principle, the theoretical analysis of the entire collision problem provided the response of the target to an external load, which is presumed to be completely elastic except for the formation of the crater, can be specified. As an example of the application of these empirical relations, the response of a beam subjected to transverse impact by a spherical striker has been evaluated.

The Hopkinson bar was chosen as the mechanism for the study of contact phenomena both because of its proven utility in numerous other investigations and because its response has been carefully analyzed both theoretically and experimentally (Ref. 15, 39, 40, and 77). The presence of dispersion due to three-dimensional effects during longitudinal pulse transmission in the bar has been amply documented; however, the manifestations of this feature can be minimized by the use of a circular rod and a sufficiently large ratio of pulse length to bar diameter, a minimum value of 8 to 10 ensuring the retention of the principal characteristics of the wave (Ref. 77 and 78). Additional dispersion will be produced when the applied load is not uniformly distributed over the end face of the rod. This situation is encountered in the impact of strikers with spherical or conical tips; the initial transient is now a spherical dilatation wave that, upon successive reflections from the lateral boundaries, rapidly approaches the character of a plane wave but is never completely uniformly distributed across the section. A further study of these factors was thus required to determine: (1) whether surface measurements by means of bonded wire strain gages could adequately represent the shape of the pulse over the entire cross section and (2), if so, where such gages should be attached to the bar to both avoid the plastic zone at the contact point and strike a suitable compromise to minimize the dispersive effects due to the two mechanisms described.

The ballistic arrangement for all tests consisted of a horizontal air gun composed of a 3-foot-long brass tube with an inside diameter of 0.505 inch, slotted near the muzzle end. The gun was capable of firing a 0.0185-pound projectile at velocities up to 300 ft/sec upon release of air from the pressure chamber by means of a quick-acting valve (Ref. 78).

In the longitudinal impact tests, the target was either ballistically suspended or else clamped at the distal end. In most cases, the impact face of the bar was carefully positioned outside the muzzle so as to yield a condition of central normal collision, but in all experiments involving conically tipped projectiles, a rod of smaller diameter was placed inside the gun barrel to better assure attainment of the desired collision condition. The initial velocity of the projectile was determined from the outputs of either two earphones or two photocells spaced a known distance apart; alternatively, both initial and rebound projectile speeds were measured either by means of a stroboscopic camera, a commercially available Fastax camera operating up to 6,000 frames/sec, or an intermediate speed camera of special design capable of a framing rate of 130,000 sec^{-1} (Ref. 75 and 78). Except for a preliminary test, all longitudinal pulses were detected by means of bonded strain gages of the wire resistance or foil type, mounted in pairs at the same axial rod position on opposite sides of a diameter or pair of faces, and coupled so as to cancel the antisymmetric component of the pulse. The gages were connected through a potentiometric or a Wheatstone bridge circuit to a cathode-ray oscilloscope with a band pass of $1\frac{1}{2}$ cycles to 1 megacycle, where a photograph of the pulse was obtained with an estimated accuracy of 1%. The oscilloscopes were triggered by a signal produced either by the passage of the striker or by the action of the wave generated in the bar. The force scale for each record was individually calibrated by observing the effect of a shunt resistance placed across the gage circuit.

The terminal crater depth, which was needed for a comparison of the permanent approach with the value calculated from the force-indentation relations, was measured by means of a profilometer with an inherent accuracy of $\pm$ 1%, while the permanent deformation of the striker was obtained even more accurately by means of a precision micrometer. A separate check on the total compression of the Hopkinson bars indicated that this effect could be neglected in the terminal-crater measurements. In some of the later tests, the indentation history was ascertained by means of the intermediate speed camera.

A preliminary investigation designed to ascertain the magnitude of the dispersive effect and the proper interpretation of strain-gage measurements was conducted on $\frac{1}{2}$-inch square bars of 2024-T4 aluminum and cold-rolled mild steel where dispersive phenomena would be even more pronounced than in the case of a circular bar. These rods were struck centrally in the longitudinal direction by a $\frac{1}{2}$-inch-diameter steel sphere with a hardness of Rockwell C 67 at velocities ranging from 130 to 190 ft/sec (Ref. 78). Typical force-time histories obtained for various impact velocities in the steel bar are presented in Fig. 3, where the original strain record has been replotted on the basis of the relation

$$F(t) = AE\epsilon(t) \tag{48}$$

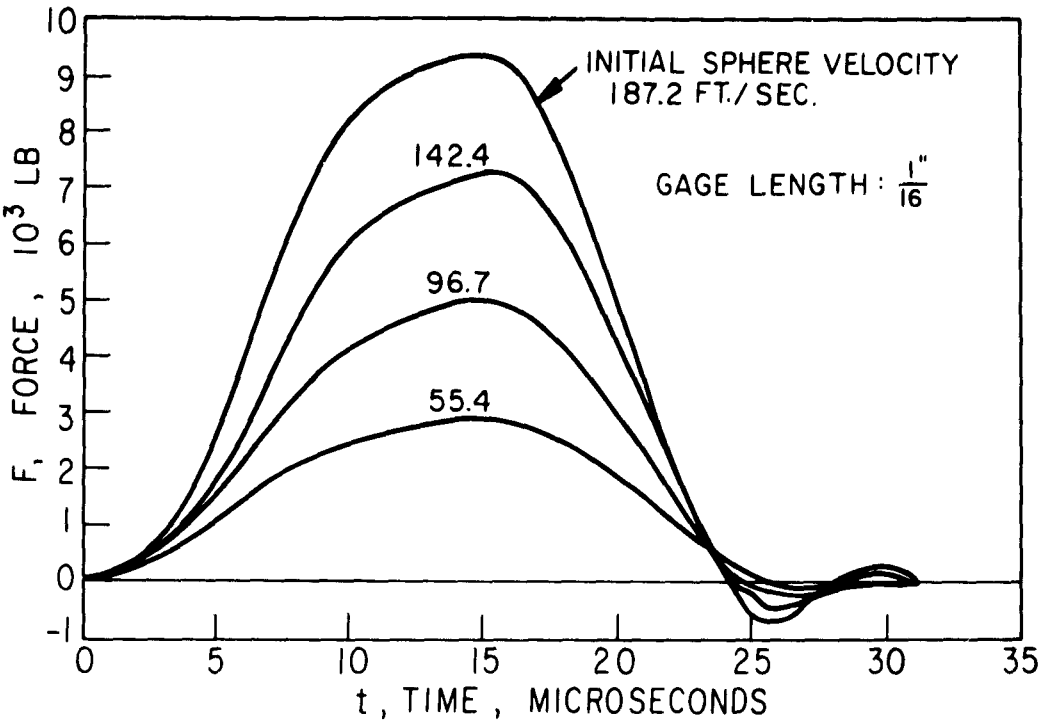

FIG. 3. Force-Time Histories Obtained From the Longitudinal Impact of a $\frac{1}{2}$-Inch-Diameter Sphere on $\frac{1}{2}$-Inch Square Bars of Cold-Rolled Mild Steel at Various Initial Velocities. Records obtained from two wire resistance gages placed on opposite faces of the bar at the same station and coupled so as to eliminate the antisymmetrical component of the pulse.

Figure 4 shows several reflections of a pulse produced in a 33-inch-long steel bar at an impact velocity of 179 ft/sec, measured by a set of wire resistance gages located 22.3 inches from the free end of the rod. The reduction of peak amplitude over twice the rod length is only 5%, the first reflected pulse being virtually a mirror image of the wave during initial transit; this indicates that three-dimensional dispersion during this interval is not significant. The dispersive effect can, however, be readily observed by the successively increasing number of oscillations at the tail of the pulse, so that optimum fidelity can only be expected during the first passage. A further indication of the combined dispersive effect is presented in Fig. 5, which compares the pulse produced in a steel bar struck at 166 ft/sec as measured by gages located 2 inches and 8 inches, respectively, from the impact point. Minor differences in the pulse shape may be noted in these records, but no further significant changes were found to occur beyond the 8-inch station. This indicates that the effect of initial dilatation has been fairly well eliminated at the nearer position, where $x/D_{equiv.}$ is of the order of 4. Recent investigations of longitudinal pulse transmission involving the embedment of gages have shown that a uniform distribution can be expected beyond a position greater than two diameters from the impact point (Ref. 80). The selection of gage positions in the longitudinal impact tests conformed to this requirement. Obviously, a gage should not be located at a station where its record would be obscured by a reflection from either end of the bar.

In order to settle the question whether a surface strain measurement could adequately represent the average strain over the cross section, a piezo-electric crystal with the same dimensions as the bar was sandwiched between two polished sections of a 2024-T4 aluminum rod. Its response was compared to that of two sets of coupled strain gages located on the rod just ahead and just behind the crystal. An X-cut quartz crystal was chosen as the transducer since its acoustic impedance was virtually the same as that of the rod; the higher signal-to-noise ratio of this device permitted an increase in the band-pass width relative to the strain-gage signal, serving as a criterion for the adequacy of the frequency cut-off level of the surface transducers. Figure 6 presents such a comparison for an impact velocity of 164 ft/sec, the force scale for the crystal having been arbitrarily adjusted to provide the correct total impulse for this test. For this gage location, approximately 20 diameters from the impact point, the two methods yield virtually coincident pulses in all respects. Although stress variations of only 3% may be expected on the basis of a theoretical analysis of the bar for the pulse length-to-diameter ratio of 10 employed here (Ref. 15), agreement in such detail was not anticipated in view of the difference in frequency response of the two systems. A further comparison of the change of momentum of the striker with the impulse determined from the strain-gage records using the static-gage factor supplied by the manufacturer and Eq. 48 indicated a discrepancy of about $\pm$ 2%, which is well within experimental error. Thus, on the basis of versatility and ease of handling and installation,

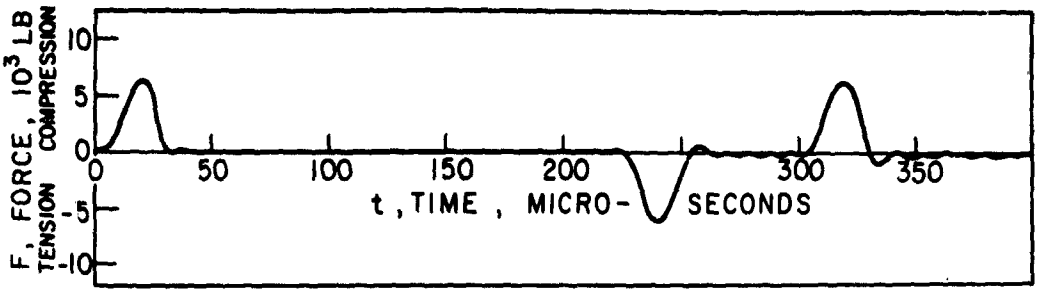

FIG. 4. Reflections of a Pulse in a $\frac{1}{2}$- by $\frac{1}{2}$- by 33-Inch Steel Rod Produced by the Longitudinal Impact of a $\frac{1}{2}$-Inch-Diameter Steel Sphere at an Impact Velocity of 179 ft/sec. Gage position: 10.7 inches from impact end.

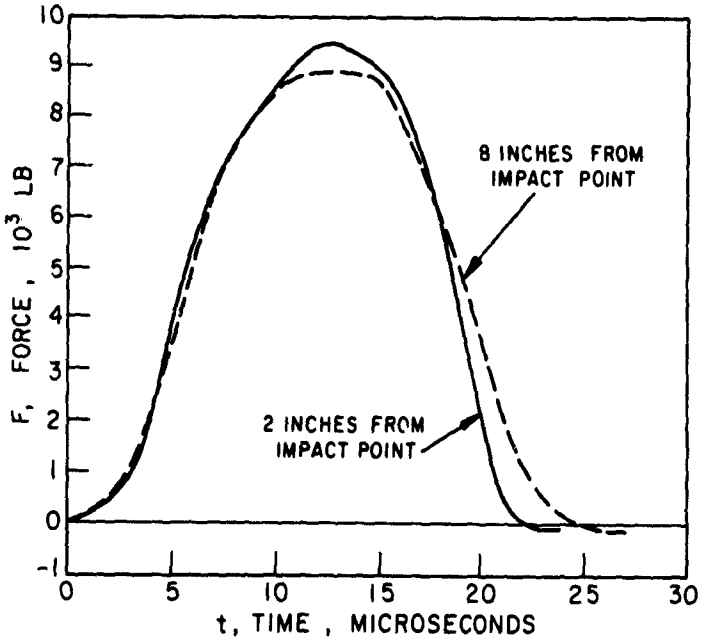

FIG. 5. Comparison of a Pulse in a $\frac{1}{2}$- by $\frac{1}{2}$- by 24-Inch Mild Steel Bar Produced by the Longitudinal Impact of a $\frac{1}{2}$-Inch-Diameter Sphere at an Impact Velocity of 166 ft/sec. Measurement performed by means of two sets of $\frac{1}{4}$-inch wire resistance gages coupled to eliminate the antisymmetric components of the pulse at stations 2 and 8 inches, respectively, from the impact point.

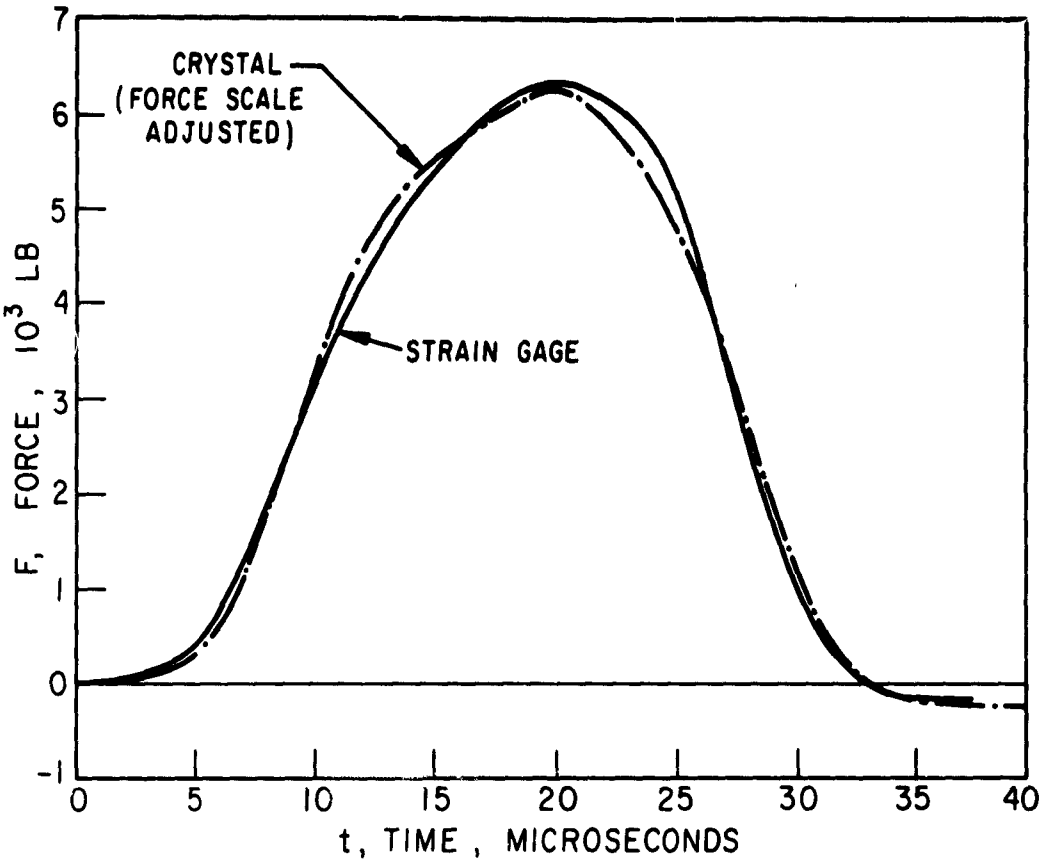

FIG. 6. Comparison of the Pulse Produced by the Impact of a $\frac{1}{2}$-Inch-Diameter Steel Sphere on a $\frac{1}{2}$-Inch-Square Bar of Aluminum at an Initial Velocity of 164 ft/sec. Measurement performed by coupled wire resistance strain gages mounted on the surface and by an X-cut quartz crystal wedged between two portions of the bar. Force scale for the uncalibrated crystal determined to correspond to the measured change of momentum of the striker.

the use of surface strain gages is to be preferred to crystal measurements, since the former exhibit an adequate frequency response, permit the direct application of the static calibration constant without correction in the range under consideration, and accurately represent the average strain over the cross section without the necessity of tailoring their shape to the bar geometry. The measurements further indicated that any gage length smaller than 10% of the pulse length yielded the correct pulse shape and total impulse. Crystal transducers should only be employed for the determination of strains below the level of 10^{-4} in/in where serious noise problems might be encountered in properly amplifying standard strain-gage signals. However, even this effect could be avoided by the use of transistorized strain gages with large gage factors that have recently become commercially available.

The conversion of force-time records of the type shown in Fig. 3 to an experimental force-indentation relation was achieved by combining the displacement relation of a striker of mass m with the one-dimensional equation of motion of the bar, Eq. 19, yielding (Ref. 71, 74, and 81)

$$\alpha = v_o t - \frac{1}{m} \int_o^t dt \int_o^t F dt - \frac{1}{\rho A c_o} \int_o^t F dt \qquad (49)$$

that can be applied stepwise over small time increments of the contact period. The use of Eq. 19 without correction factors permits an enormous simplification of the data-reduction procedure, but neglects, of course, the effects of both initial spherical dilatation and three-dimensional dispersion. In view of the preliminary experiments, the influence of these characteristics was believed to be small as far as the gross features of the pulse propagation in the bar was concerned, provided the measuring station was suitably located and the pulse was sufficiently long. Nevertheless, an inspection of the strain-gage records revealed a noticeable rounding of both the initial and terminal portions of the pulse that is largely attributable to the dispersive features of the rod and is partly induced by the higher modes of symmetric propagation (Ref. 74). The definition of the force-indentation relation was found to be highly sensitive to the precise delineation of the start of the pulse; to eliminate the influence of dispersion, the steeply rising portion of each pulse was extrapolated linearly back to the base line in the analysis of the records. As a consequence of this procedure, the final values of the approach as calculated from the strain histories and those measured subsequent to the tests were found to be in excellent accord. The loss in pulse area incurred by this extrapolation affected the impulse by less than 1% and produced a negligible shift of the calculated force-indentation relations. The dispersive manifestations at the end of the record, involving both a rounding of the descending part of the pulse and subsequent high-frequency oscillations, did not exert a significant influence on the character of the calculated curves and were thus neglected in most instances. In some tests involving soft

metals, such as lead, the strain gages were subjected to a permanent set as indicated by a shift in the base line of their records; in all such cases, the base-line position could be properly adjusted so as to permit the use of data obtained under these conditions.

The use of Eq. 49 also neglects the vibrations of the striker that, in the case of a spherical projectile, has been justified on theoretical grounds (Ref. 2). However, for a cylindrical striker with a conical head, a similar analysis cannot be performed even with the crudest types of assumptions, and the magnitude of the vibrational energy in such a body can consequently not be readily estimated. The predictions of Eq. 49 for this case can, however, be compared with an analysis developed for the longitudinal impact of bars with rounded ends which accounts for successive reflections of plane elastic waves in the projectile by considering the distal end of the striker as a free surface and the impact face as rigid (Ref. 81). This leads to the relation

$$\alpha = v_o t - \frac{1}{\rho_2 A_2 c_{o_2}} \int_o^t F dt - \frac{1}{\rho_1 A_1 c_{o_1}} \int_o^t \left[F + 2 \sum_{i=1}^{k} F < t - \frac{2iL_1}{c_{o_1}} > \right] dt \quad (50)$$

where subscripts 1 and 2 denote the projectile and the bar, respectively, $k = 2L_1/c_{o_1}\tau$ defines the number of double wave reflections in the equivalent striker length L_1 during pulse duration τ, and $F < t - 2iL_1/c_{o_1} >$ delineates successive reflections at the impact point, an additional term appearing in the integral for each return of the wave to the contact surface. While the actual conditions at this position will differ considerably from those assumed in the derivation of Eq. 50, the postulated situation represents the case of maximum vibratory energy storage in the striker and thus permits, in conjunction with Eq. 49, the establishment of upper and lower bounds concerning the magnitude of this effect.

In addition to theoretical justification, the validity of the assumptions inherent in the data-conversion process is strongly supported by the excellent agreement noted between the change of momentum of the strikers and the measured impulse in the rod on one hand, and the measured and calculated values of the terminal approach on the other. Further corroboration is provided by the good correspondence exhibited between the calculated and photographically observed indentation histories. This is exemplified by Fig. 7 that shows the experimental force-indentation curves and those determined from strain-gage records for the impact on a $\frac{1}{2}$-inch-diameter steel rod of both a $\frac{1}{2}$-inch-diameter hard steel sphere and a $\frac{1}{2}$-inch-diameter cylindrical projectile of the same mass and a conical tip of $2\beta = 120$ degrees at about the same initial velocity of 150 ft/sec. Figure 8 presents a comparison of results obtained from a strain-time record by means of Eq. 49 and 50, respectively, for the impact of a similar conical projectile at a velocity of 176 ft/sec and the corresponding photographic record. The two calculated curves are nearly coincident, indicating that the vibrational effects in

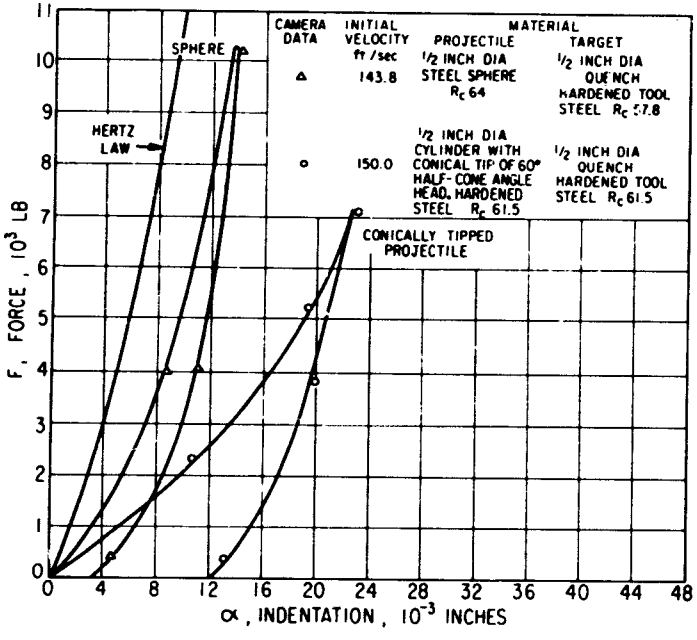

FIG. 7. Comparison of the Force-Indentation Curves for the Longitudinal Impact of a ½-Inch-Diameter Hard Steel Sphere and a Hard Steel Cylindrical Projectile With a Conical Tip of Half-Angle β = 60 Degrees Against a Bar of Quench-Hardened Tool Steel at a Velocity of 150 ft/sec. Indentation calculated from Eq. 49.

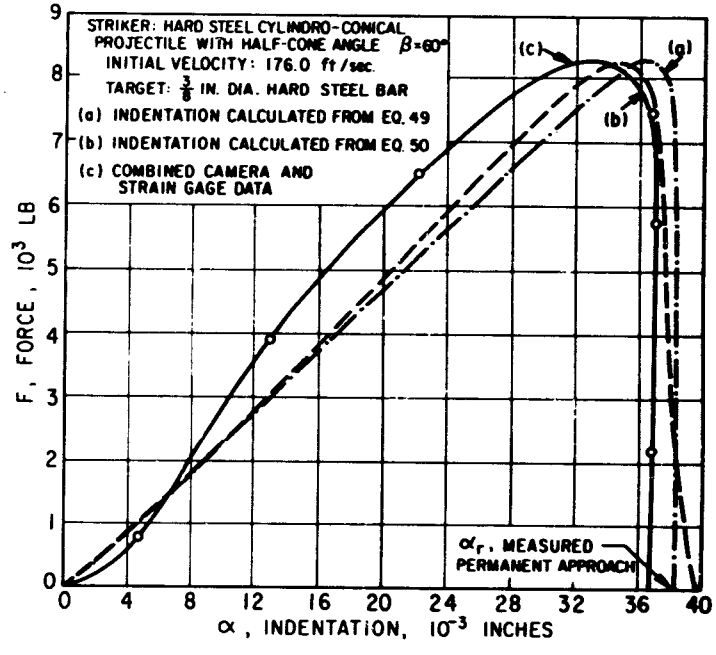

FIG. 8. Force-Indentation Curves Calculated from Eq. 49 and 50, Respectively, and Observed by Means of a Framing Camera for the Impact of a Cylindrical Projectile With a Conical Tip of Half-Angle β = 60 Degrees Against the Plane End of a Hard Steel Bar at a Velocity of 176 ft/sec.

the cylindro-conical striker can indeed be neglected, and that Eq. 49 will permit a satisfactory reduction of the strain-gage data. The permissibility of treating the projectile as a nonvibrating mass could also have been argued on the basis that several passages of the elastic wave must occur during the contact period, producing a state of quasi-equilibrium in the striker, under which circumstances this body can be treated as a nonresonating, albeit deformable mass. All curves presented in Fig. 8 are in excellent accord with the subsequent measured value of the permanent indentation of α_r = 0.0372 inch, providing an additional check on the justification for the use of Eq. 49 in all subsequent data analyses.

The static stress-strain curves and other relevant mechanical properties of two tool steels of different hardness, mild cold-rolled steel, and two types of aluminum-alloy targets are presented in Fig. 9 (Ref. 74), partially annealed tool steel, and lead comprising other target materials. Dynamic tests were carried out by means of the Hopkinson bar technique in the velocity range from 30–300 ft/sec with $\frac{1}{2}$-inch-diameter spherical steel or brass projectiles, $\frac{1}{2}$-inch-diameter strikers consisting of a cylindrical base and a conical tip with angles ranging from 2β = 20 degrees to 2β = 160 degrees, composed variously of 2024-T4 aluminum, commercial brass, or tool steel of various hardness, or similar conically headed steel bullets with a total angle of 60 degrees, but hemispherically rounded at the tip with radii varying between 0.025 and 2.0 inches. Corresponding static force-indentation curves were obtained from measurements of the slow compression in a standard testing machine of two short $\frac{1}{2}$-inch-diameter blocks of the target material that were separated by the appropriate projectile.

The static and dynamic force-indentation relations as well as the predictions of the Hertz law, Eq. 39, have been plotted in Fig. 10–14 for the collision of steel projectiles with the target materials characterized in Fig. 9 (Ref. 74 and 75). The dynamic approach and recovery curves for all target materials subjected to the impact of such strikers have been summarized in Fig. 15; the compression phase for all substances except 2024-T4 aluminum could be represented by a single line over the entire velocity range employed. Figure 16 presents additional results for the impact of brass spheres against tool steel and the collision of a steel sphere with a bar composed of two end sections of mild steel sweated onto a center portion of quench-hardened tool steel where the strain gages were located. The latter arrangement was dictated by the magnetostrictive properties exhibited by mild steel that produce a spurious signal in strain-gage records upon passage of a pressure pulse induced by the field effect of the bar on the external wiring system.

The variation of the compression phase of the force-indentation relations with initial velocity obtained by means of conical strikers was considered to be sufficiently small except for the case of the minimum total cone angle of 20 degrees so that the dynamic results could also be represented by a single curve, as indicated in Fig. 17. The static and dynamic data for identical projectile and target materials involving conically tipped projectiles of 60- and 120-degree total angle are compiled in

Fig. 18 and 19, and similar results are exhibited in Fig. 20 and 21 for strikers and bars of differing composition. The greater scatter of the curves at differing initial velocities for the smallest cone angle of $2\beta = 20$ degrees involved in these tests is illustrated in Fig. 22 and 23. A sequence of runs involving conically headed tool steel projectiles with varying cone angles, but identical mass, fired with the same initial velocity against tool steel rods yielded the information shown in Fig. 24. Experiments carried out under similar conditions with hemispherically tipped cylindro-conical slugs of both hardened and annealed tool steel against similar target materials resulted in the data presented in Fig. 25 and 26.

A comparison of the static and dynamic force-indentation curves for spherical projectiles reveals a virtual coincidence for the case of quench-hardened tool steel; a force up to 25% larger is required to produce the same indentation under dynamic conditions for annealed tool steel, aluminum, and lead, while an increase of 50% is exhibited for cold-rolled mild steel. The results for the hard tool steel are also in excellent agreement with the predictions of Eq. 39, whereas large discrepancies can be observed between values so computed and the experimental results for all other materials. This apparent anomaly arises from the fact that the impact process in the case of the hard steel was primarily elastic for the initial velocity range employed, as evidenced by a crater recovery of the order of 50%. This observation vindicates the use of the Hertz relation under the proper circumstances even when some permanent set is produced, but also denies its application to those cases of relatively small restitution that were observed with other materials. The energy required for the production of the permanent indentation in the hard steel is thus only a small percentage of the initial kinetic energy. At velocities above the range under investigation, the differences in the three sets of curves for this substance would undoubtedly increase in a manner similar to that exhibited by the other target materials. The larger increase in force observed for the cold-rolled mild steel might have been expected on the basis of the demonstrated higher strain-rate sensitivity of this material, whose elastic limit under dynamic conditions reportedly can be raised relative to its static value by a factor ranging from about 1.2 to more than 3, depending upon composition and loading rate (Ref. 13 and 82).

Corresponding differences between static and dynamic data for conically tipped projectiles indicate an increase of the force ranging from 25 to 50% for the tool steel and aluminum targets and the various strikers employed. The difference in the percentage increase of the force for the different geometries of the projectile may be due to the greater inertial resistance of the target that is accelerated more rapidly at the tip of a conical bullet than at the point of maximum penetration of a sphere whose radius is large compared with the crater depth. The results obtained with conical indenters cannot be logically compared with the predictions of the Hertz law, since the latter is based on a reversible process involving contact surfaces defined by equations of the second degree, and both of these requirements were seriously violated in this sequence of tests.

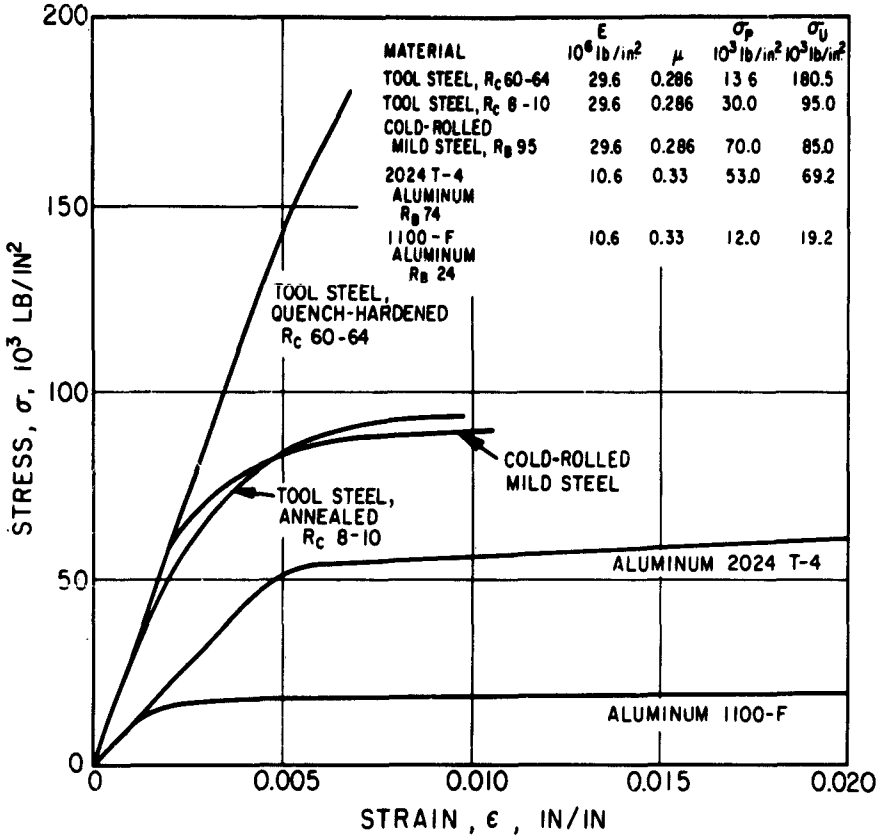

FIG. 9. Static Stress-Strain Curves and Mechanical Properties of Five Target Materials. E, modulus of elasticity, 10^6 lb/in^2; μ, Poisson's ratio; σ_p, static proportional limit, 10^3 lb/in^2; σ_u, static ultimate strength, 10^3 lb/in^2; R_C, Rockwell hardness, scale C.

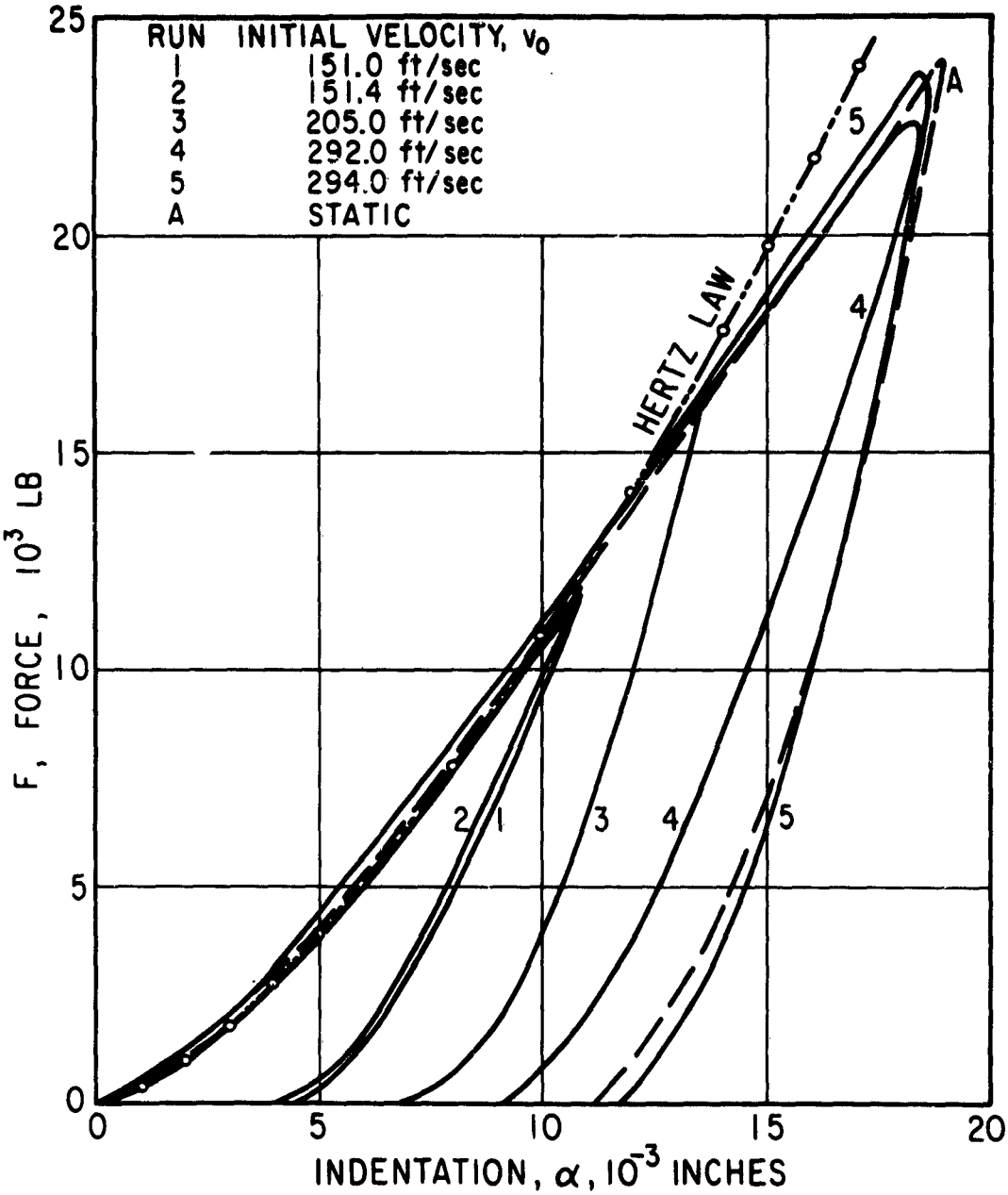

FIG. 10. Static and Dynamic Force-Indentation Curves for Quench-Hardened Tool Steel, R_C 60-64. Indenter, ½-inch-diameter hard steel sphere; target, ½-inch-diameter bar.

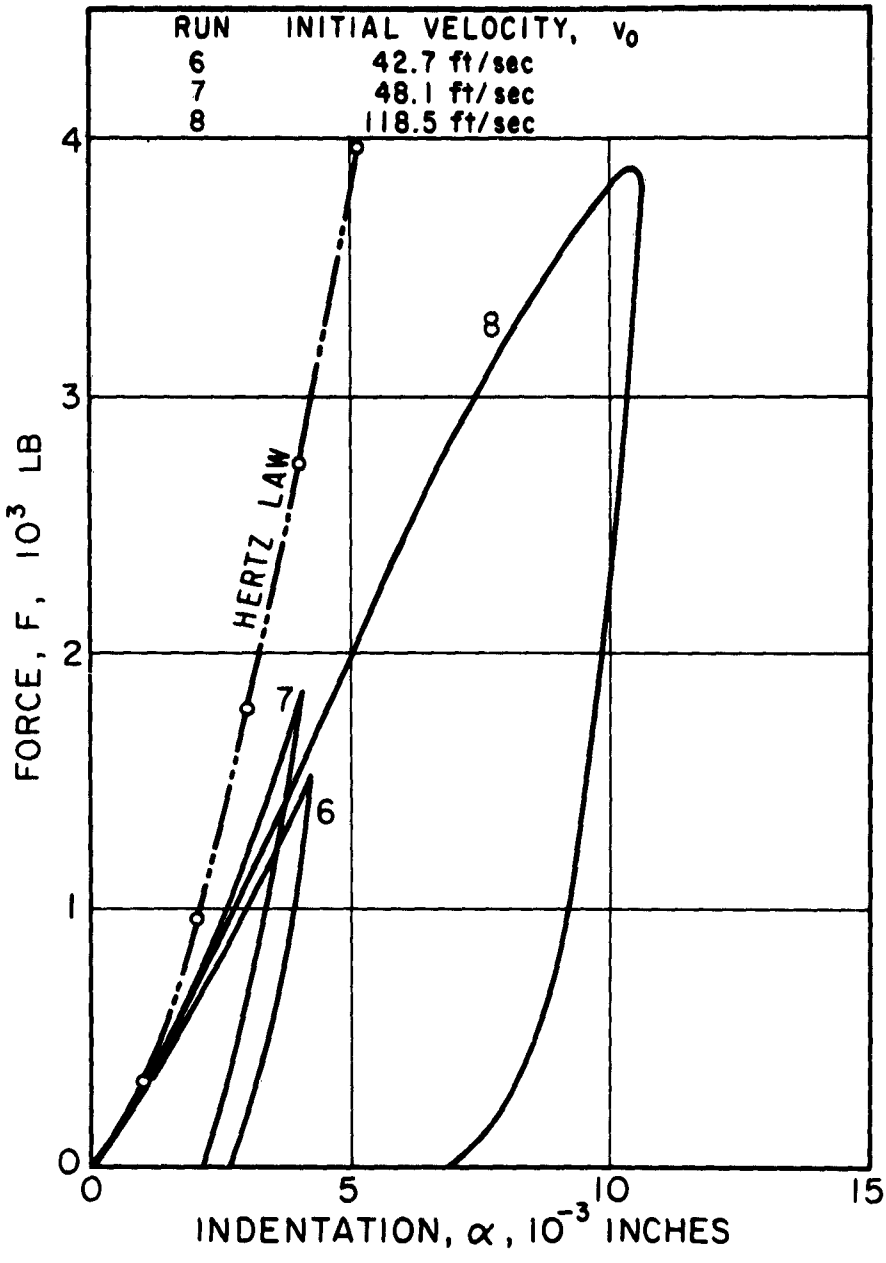

FIG. 11. Dynamic Force-Indentation Curves for Annealed Tool Steel, R_C 6–12. Indenter, $\frac{1}{2}$-inch-diameter hard steel sphere; target, $\frac{1}{2}$-inch-diameter bar.

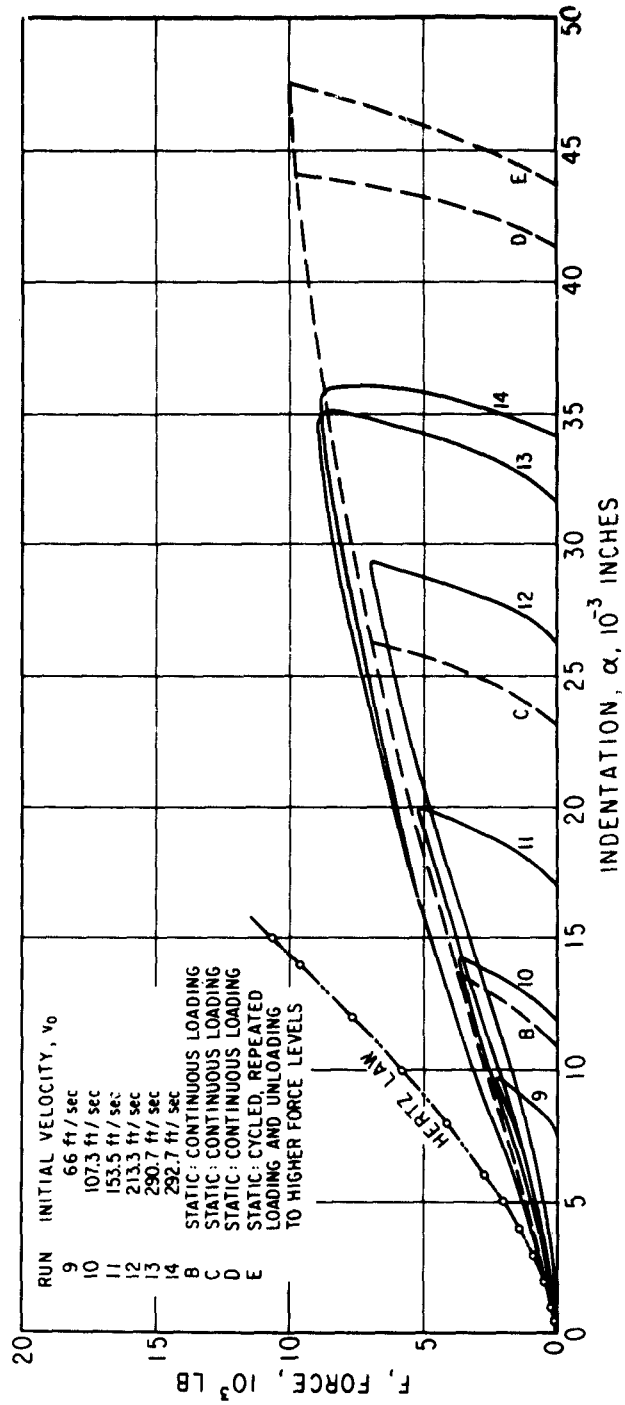

FIG. 12. Static and Dynamic Force-Indentation Curves for 2024-T4 Aluminum, R_B 74. Indenter, ½-inch-diameter hard steel sphere; target, ½-inch-diameter bar.

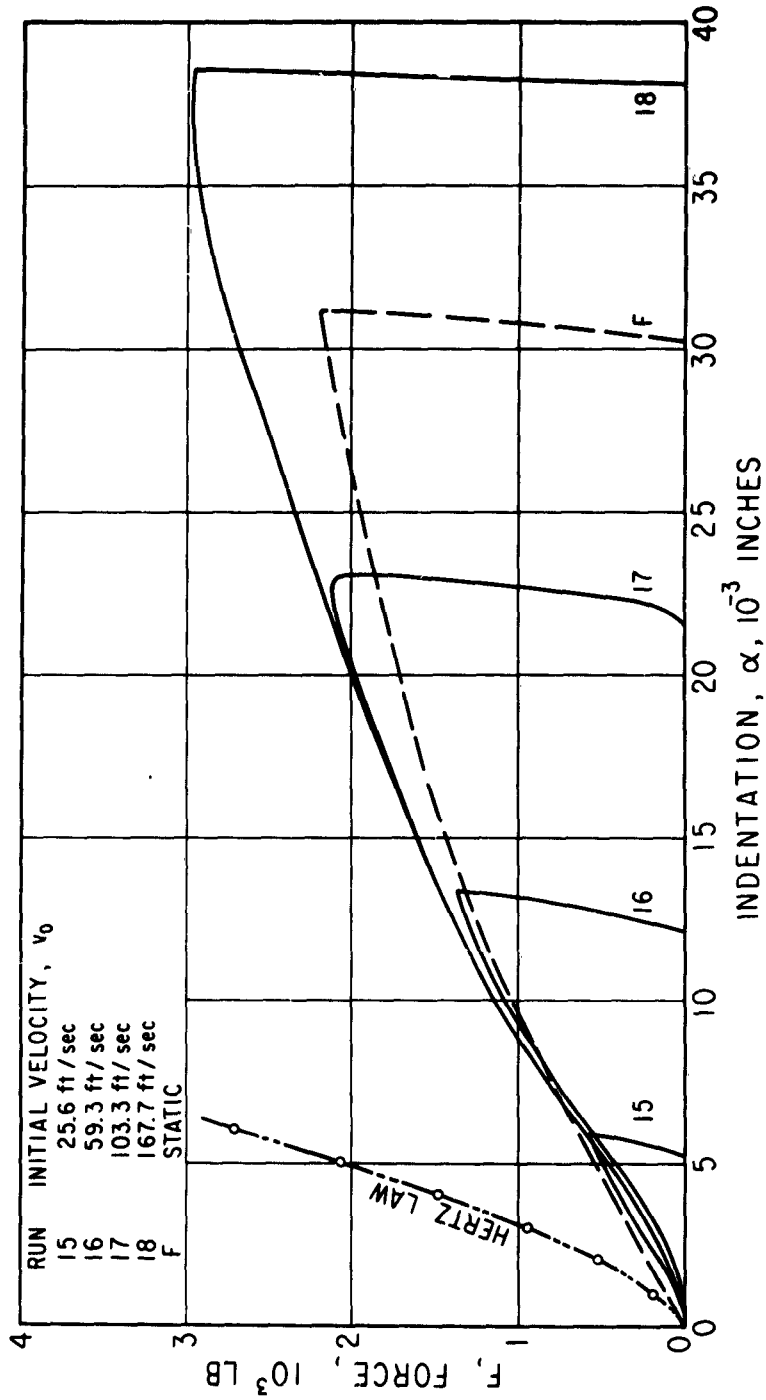

FIG. 13. Static and Dynamic Force-Indentation Curves for 1100-F Aluminum, R_B 24. Indenter, ½-inch-diameter hard steel sphere; target, ½-inch-diameter bar.

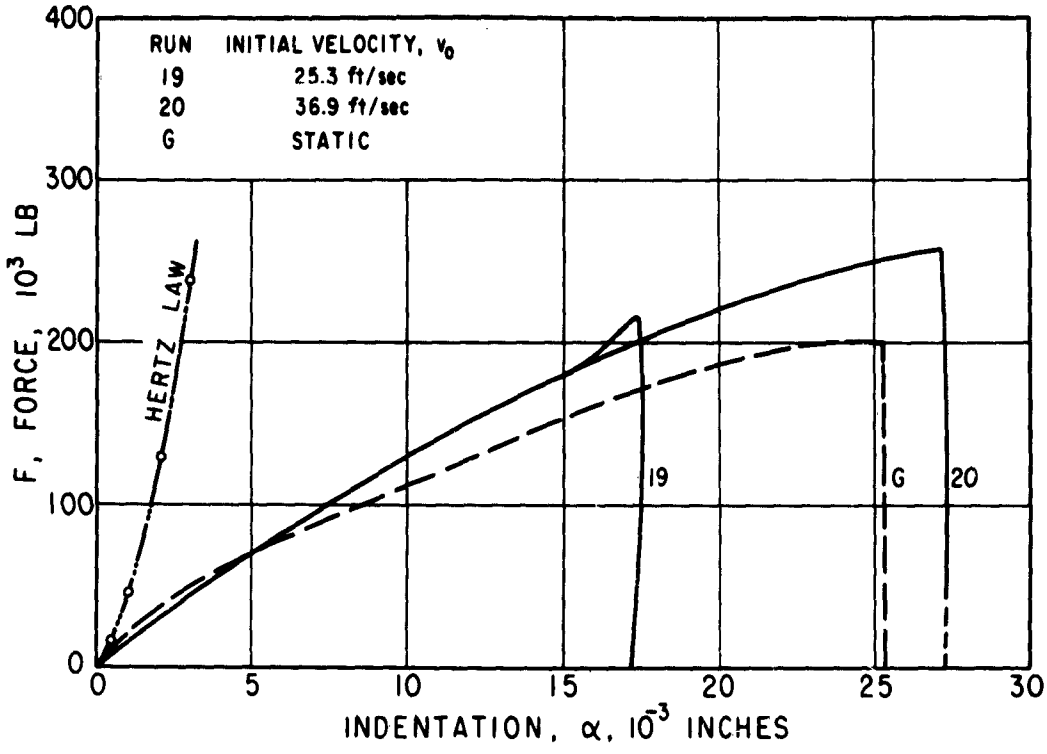

FIG. 14. Static and Dynamic Force-Indentation Curves for Extruded Lead. Indenter, $\frac{1}{2}$-inch-diameter hard steel sphere; target, $\frac{1}{2}$-inch diameter bar.

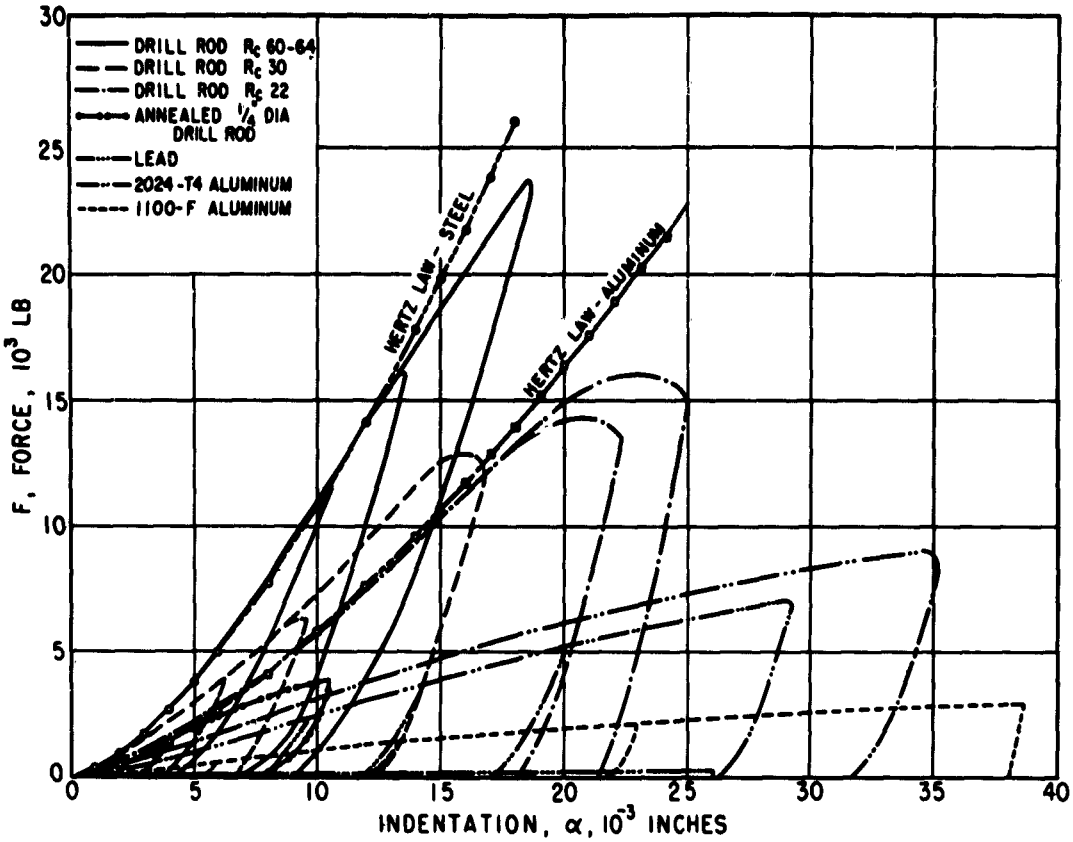

FIG. 15. Dynamic Force-Indentation Curves for the Longitudinal Impact of a $\frac{1}{2}$-Inch-Diameter Hard Steel Sphere Against the Plane End of $\frac{1}{2}$-Inch-Diameter Bars of Various Metals.

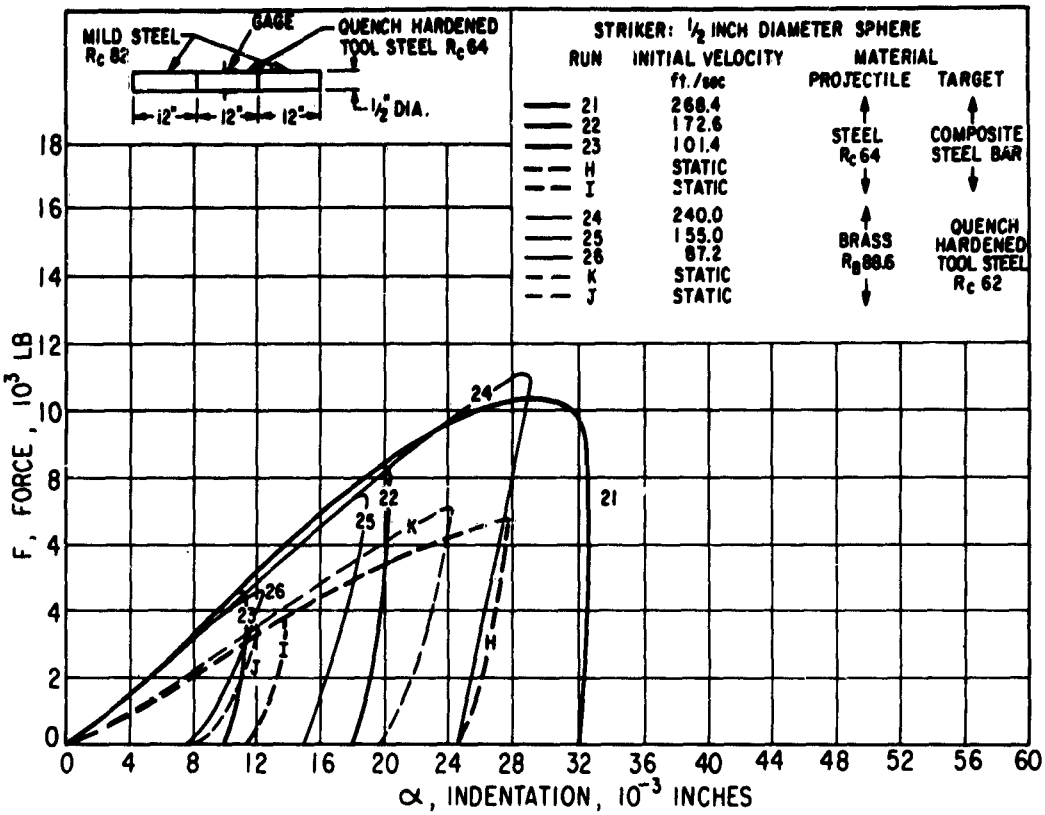

FIG. 16. Static and Dynamic Force-Indentation Curves for the Impact of a ½-Inch-Diameter Sphere of Brass and Hard Steel Against the Plane End of ½-Inch-Diameter Bars of Steel.

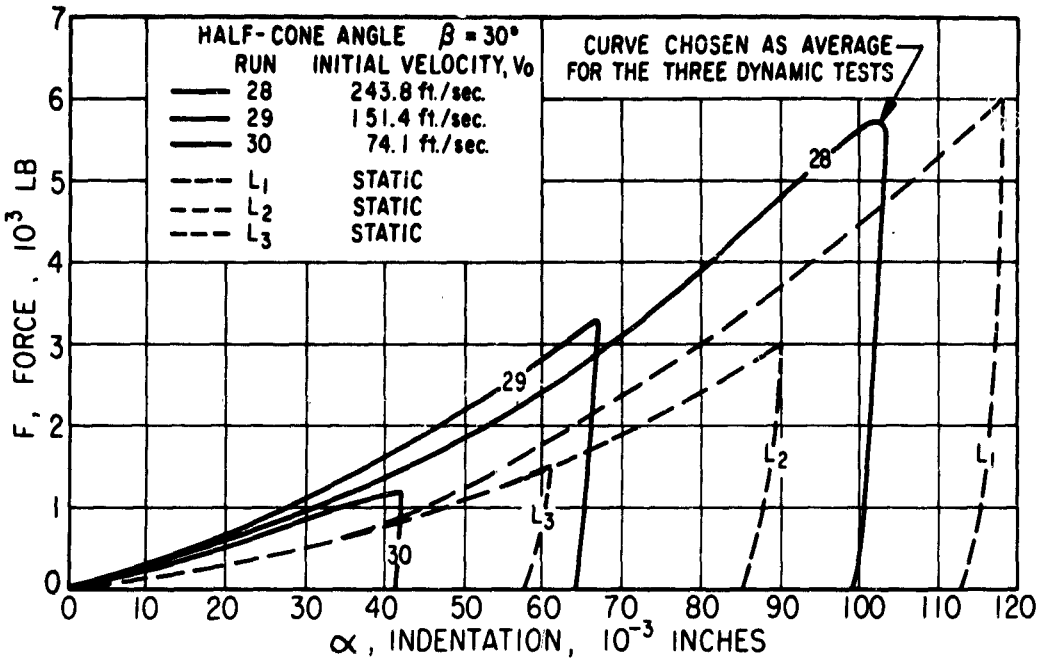

FIG. 17. Typical Variation of Static and Dynamic Force-Indentation Curves With Peak Load and Initial Velocity. Indenter, cylindro-conical slugs of annealed tool steel with half-cone angle β = 30 degrees; target, 3/8-inch-diameter annealed tool steel bar.

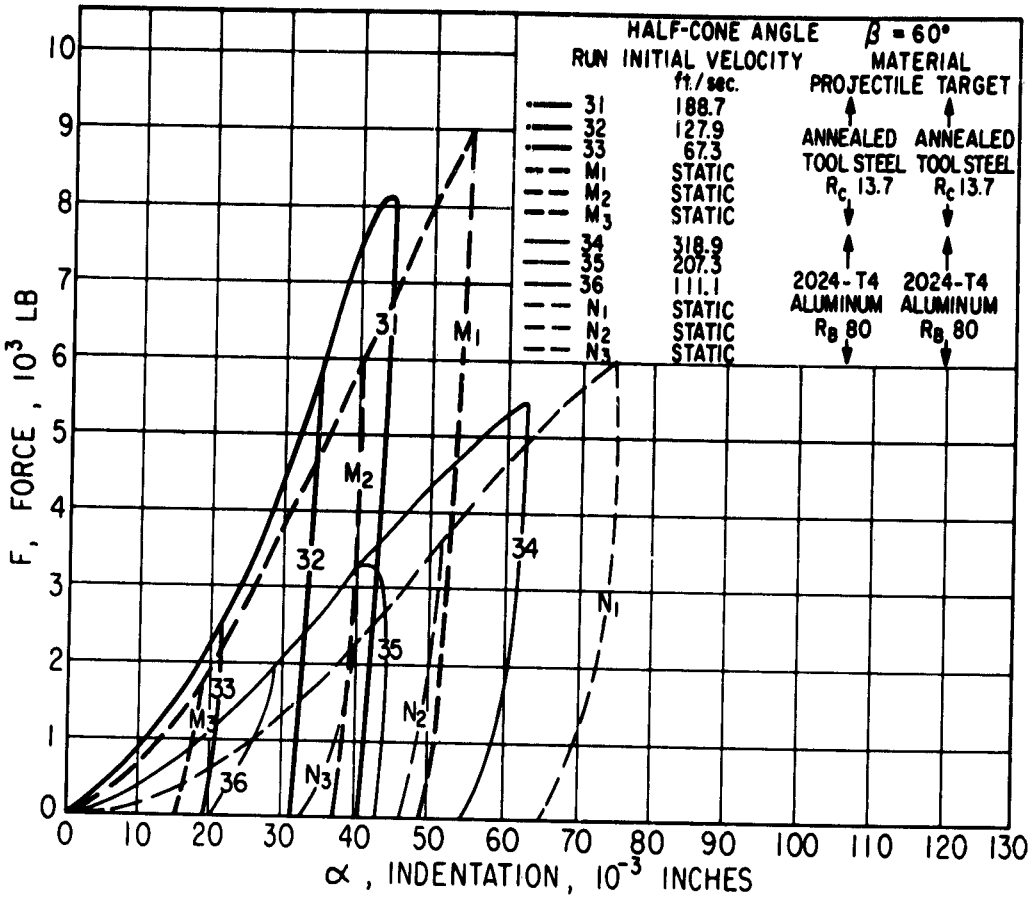

FIG. 18. Static and Dynamic Force-Indentation Curves for Conically Headed Projectiles of Annealed Tool Steel and and 2024-T4 Aluminum Striking 3/8-Inch-Diameter Bars of Identical Materials.

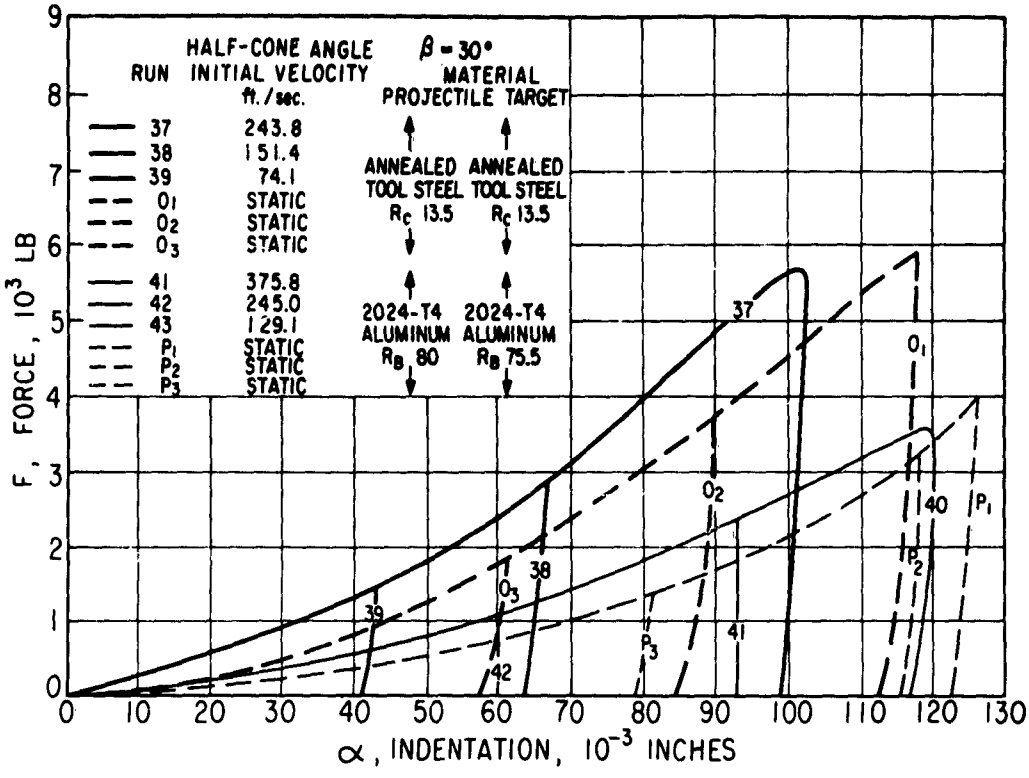

FIG. 19. Static and Dynamic Force-Indentation Curves for Conically Headed Projectiles of Annealed Tool Steel and 2024-T4 Aluminum Striking 3/8-Inch-Diameter Bars of Identical Materials.

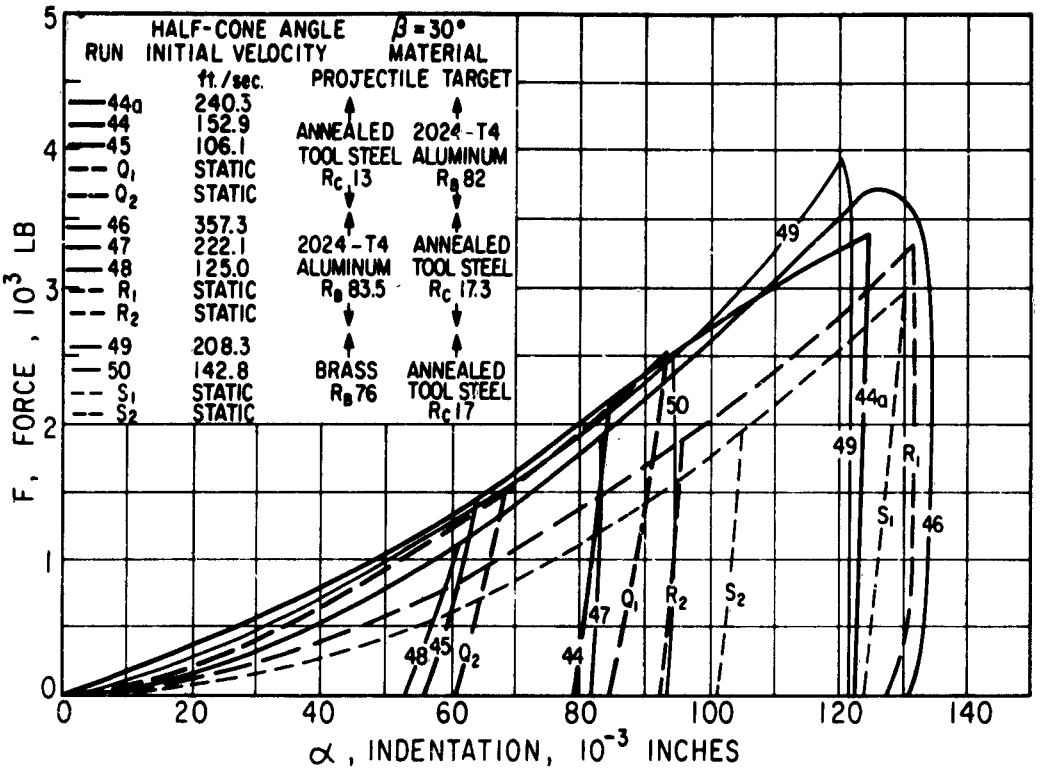

FIG. 20. Static and Dynamic Force-Indentation Curves for Conically Headed Projectiles of Annealed Tool Steel, 2024-T4 Aluminum and Brass Striking 3/8-Inch-Diameter Bars of Dissimilar Target Materials.

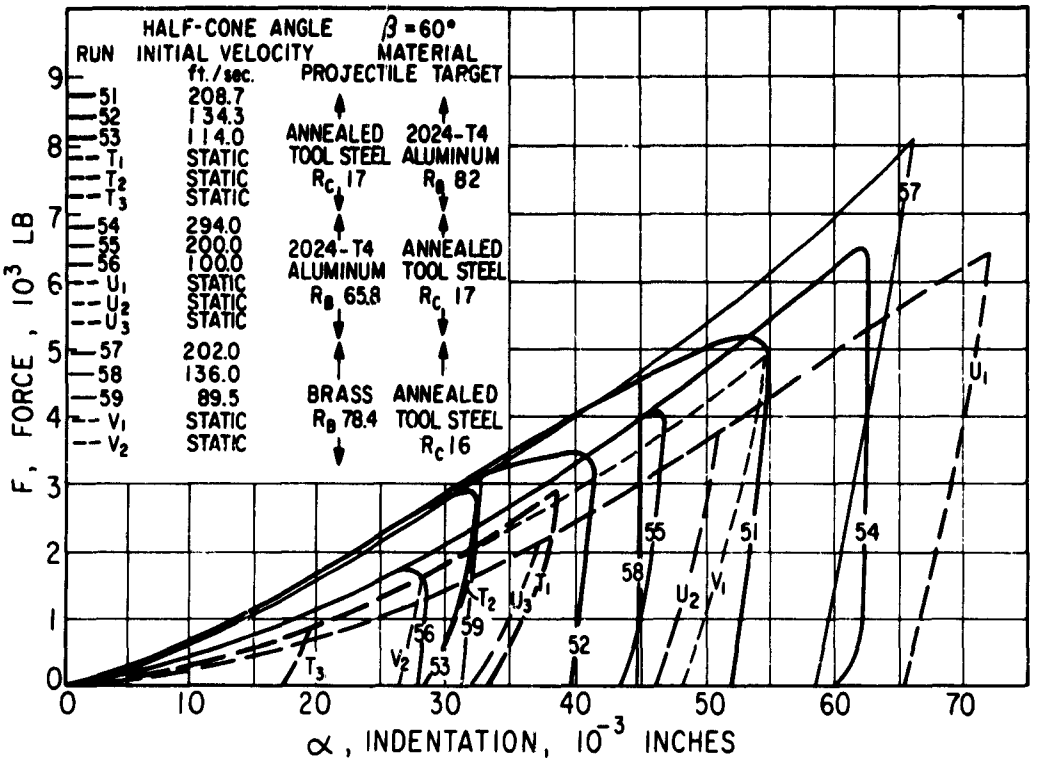

FIG. 21. Static and Dynamic Force-Indentation Curves for Conically Headed Projectiles of Annealed Tool Steel, 2024-T4 Aluminum and Brass Striking 3/8-Inch-Diameter Bars of Dissimilar Target Materials.

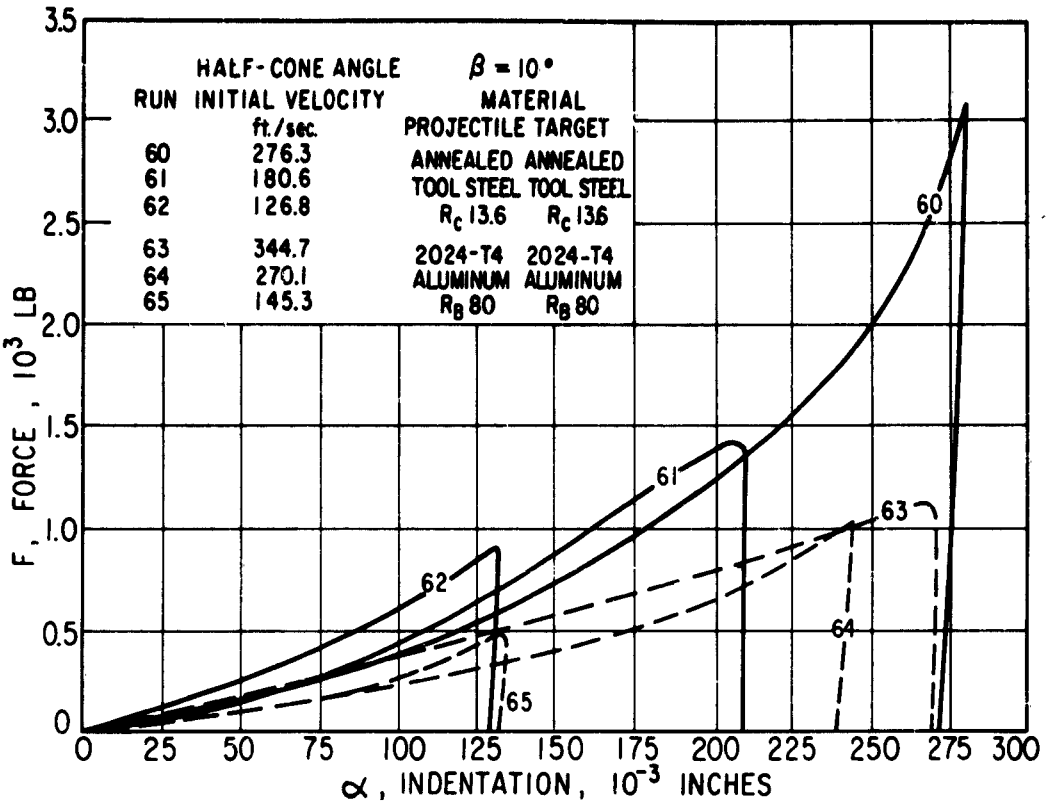

FIG. 22. Dynamic Force-Indentation Curves for Conically Headed Projectiles of Annealed Tool Steel and 2024-T4 Aluminum Striking 3/8-Inch-Diameter Bars of Identical Target Materials.

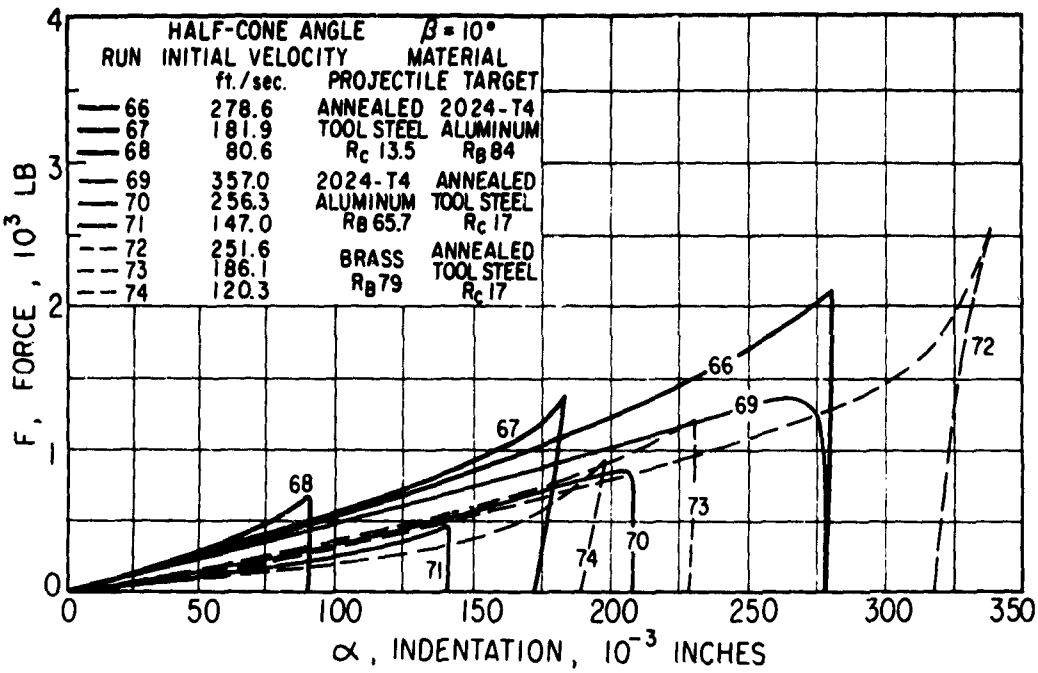

FIG. 23. Dynamic Force-Indentation Curves for Conically Headed Projectiles of Annealed Tool Steel, 2024-T4 Aluminum and Brass Striking 3/8-Inch-Diameter Bars of Dissimilar Target Materials.

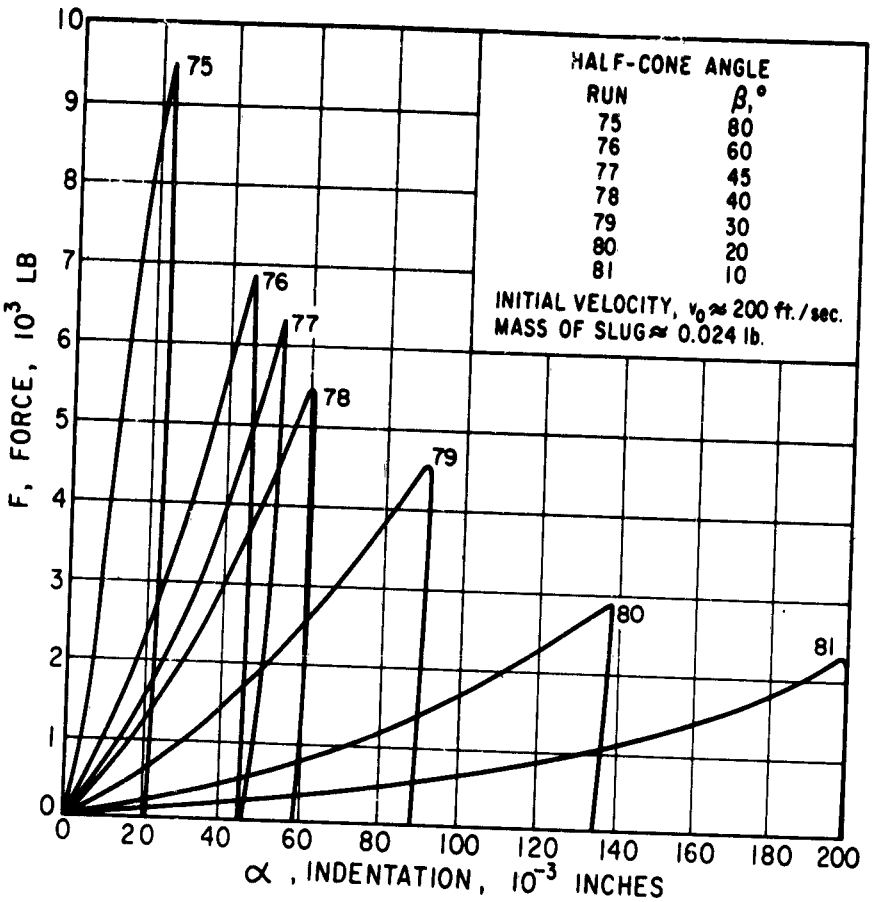

FIG. 24. Dynamic Force-Indentation Curves for the Impact of an Annealed Tool Steel Cylindro-Conical Slug of Constant Mass With Half-Cone Angles Ranging from 10–80 Degrees Against the Plane End of an Annealed Tool Steel Rod.

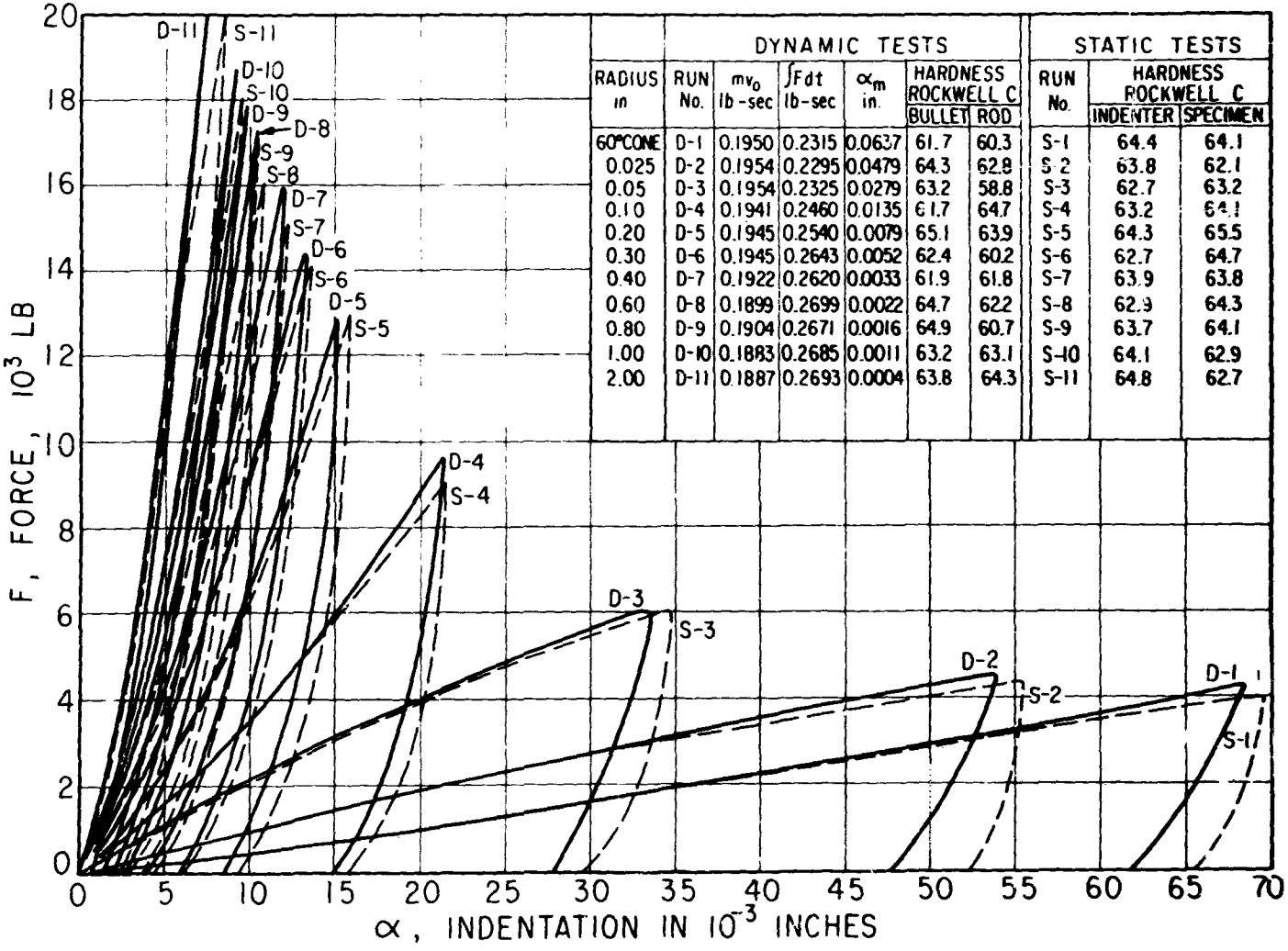

RADIUS in	RUN No.	DYNAMIC TESTS mv_0 lb-sec	$\int Fdt$ lb-sec	α_m in.	HARDNESS ROCKWELL C BULLET	HARDNESS ROCKWELL C ROD	STATIC TESTS RUN No.	HARDNESS ROCKWELL C INDENTER	HARDNESS ROCKWELL C SPECIMEN
60°CONE	D-1	0.1950	0.2315	0.0637	61.7	60.3	S-1	64.4	64.1
0.025	D-2	0.1954	0.2295	0.0479	64.3	62.8	S-2	63.8	62.1
0.05	D-3	0.1954	0.2325	0.0279	63.2	58.8	S-3	62.7	63.2
0.10	D-4	0.1941	0.2460	0.0135	61.7	64.7	S-4	63.2	64.1
0.20	D-5	0.1945	0.2540	0.0079	65.1	63.9	S-5	64.3	65.5
0.30	D-6	0.1945	0.2643	0.0052	62.4	60.2	S-6	62.7	64.7
0.40	D-7	0.1922	0.2620	0.0033	61.9	61.8	S-7	63.9	63.8
0.60	D-8	0.1899	0.2699	0.0022	64.7	62.2	S-8	62.9	64.3
0.80	D-9	0.1904	0.2671	0.0016	64.9	60.7	S-9	63.7	64.1
1.00	D-10	0.1883	0.2685	0.0011	63.2	63.1	S-10	64.1	62.9
2.00	D-11	0.1887	0.2693	0.0004	63.8	64.3	S-11	64.8	62.7

FIG. 25. Static and Dynamic Force-Indentation Curves for the Impact of Quench-Hardened Tool Steel Cylindro-Conical Slugs of Half-Cone Angle β = 30 Degrees and Hemispherical Tip Radii Ranging From 0.025-2.0 Inches Against the Plane End of a Quench-Hardened 3/8-Inch-Diameter Tool Steel Bar. Initial velocity, 113 ft/sec.

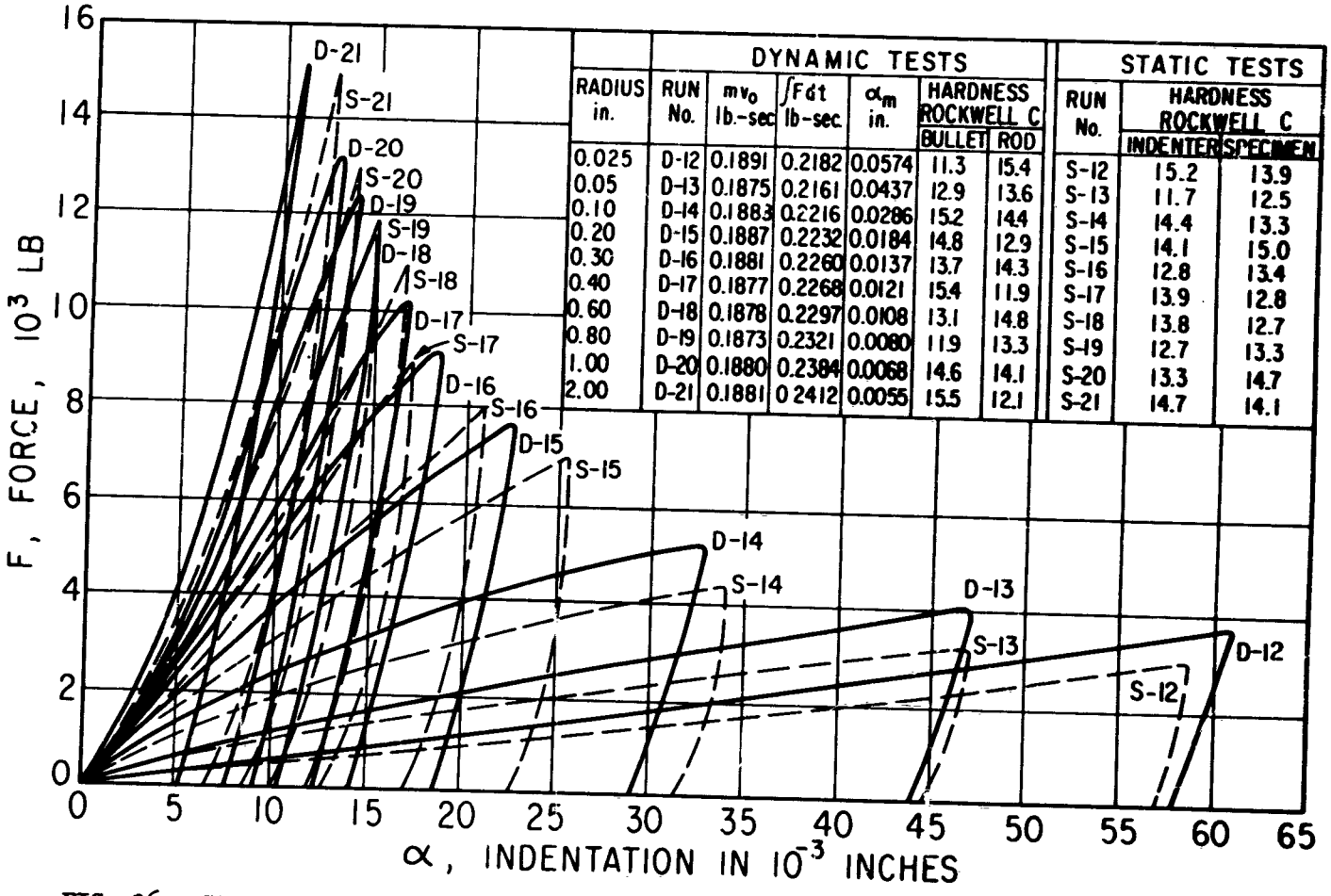

RADIUS in.	DYNAMIC TESTS RUN No.	mv_o lb.-sec	$\int F dt$ lb-sec.	α_m in.	HARDNESS ROCKWELL C BULLET	ROD
0.025	D-12	0.1891	0.2182	0.0574	11.3	15.4
0.05	D-13	0.1875	0.2161	0.0437	12.9	13.6
0.10	D-14	0.1883	0.2216	0.0286	15.2	14.4
0.20	D-15	0.1887	0.2232	0.0184	14.8	12.9
0.30	D-16	0.1881	0.2260	0.0137	13.7	14.3
0.40	D-17	0.1877	0.2268	0.0121	15.4	11.9
0.60	D-18	0.1878	0.2297	0.0108	13.1	14.8
0.80	D-19	0.1873	0.2321	0.0080	11.9	13.3
1.00	D-20	0.1880	0.2384	0.0068	14.6	14.1
2.00	D-21	0.1881	0.2412	0.0055	15.5	12.1

STATIC TESTS RUN No.	HARDNESS ROCKWELL C INDENTER	SPECIMEN
S-12	15.2	13.9
S-13	11.7	12.5
S-14	14.4	13.3
S-15	14.1	15.0
S-16	12.8	13.4
S-17	13.9	12.8
S-18	13.8	12.7
S-19	12.7	13.3
S-20	13.3	14.7
S-21	14.7	14.1

FIG. 26. Static and Dynamic Force-Indentation Curves for the Impact of Annealed Tool Steel Cylindro-Conical Slugs of Half-Cone Angle β = 30 Degrees and Hemispherical Tip Radii Ranging From 0.025-2.0 Inches Against the Plane End of an Annealed 3/8-Inch-Diameter Tool Steel Bar. Initial velocity, 113 ft/sec.

Inspection of Fig. 10–15 reveals that none of the metals subjected to impact by a spherical projectile exhibited a linear force-indentation curve; thus, a constant flow pressure does not prevail during the entire indentation process, and Eq. 44 cannot be applied except as an approximation. Table 1 lists such average values of the mean static and dynamic flow pressures obtained from the present series of tests and from other investigations (Ref. 66 and 71). Good agreement exists between corresponding values, particularly with respect to the ratio of dynamic to static pressures, in spite of the differences in experimental arrangement and properties of the materials examined. However, the inital portion of all indentation diagrams displays an upward curvature similar to that prescribed by Eq. 39; all materials except the hard steel also exhibit a concave downward curvature at larger values of the indentation. This curvature reversal cannot be expressed empirically by a relation of the form of Eq. 42.

The validity of the assumption of a constant flow pressure for the impact of conically tipped strikers, leading to Eq. 45 and 47, can be checked by an examination of the results presented in Fig. 17–24. A logarithmic plot of these data indicates that all tests can be represented by Eq. 42 during the compression phase, but with exponents ranging from $n = 1.25$ to $n = 1.75$ that differ from the value of $r = 2$ derived on the basis of a constant value of p_o. This hypothesis should consequently be replaced by an expression in which the dependence of mean flow pressure upon rate of indentation is recognized. Furthermore, the mean resistive pressure at the instant of maximum penetration, computed from Eq. 45, was found to decrease with increasing impact velocity for otherwise identical collision conditions. This trend cannot be explained on the basis of a strain-rate effect, which would produce a contrary result, but must instead be attributed to a change in the frictional mechanism at higher indentation speeds. The assumption of a constant frictional coefficient, embodied in Eq. 46 and 47, will certainly result in a grossly oversimplified description of the process.

The data shown in Fig. 24 indicate that, for otherwise identical impact conditions, an increase in cone angle produces a higher peak force and a smaller permanent conical crater. This result is expected since a hard indenter of smaller cone angle will encounter less penetration area and hence less resistance, while a soft indenter can deform more readily the smaller the cone angle. An opposite conclusion was reached in another investigation (Ref. 72) where, however, the experimental arrangement was quite different and the collision velocity much lower. A simple empirical relation could not be found to describe the envelope of the curves of Fig. 24 in terms of the cone angle 2β. This situation prevents the establishment of a quantitative connection between corresponding tests involving spherical and conically tipped indenters. However, it may be observed from Fig. 7 that, for comparable initial velocities, a conical striker develops a considerably greater penetration at a lower peak force than a sphere of identical mass, and that the mean pressure at the instant of maximum penetration for the cone is considerably larger, of the order of

TABLE 1. Comparison of Average Flow Pressures for Present Experiments with Those Determined by Other Investigators

Average flow pressure, lb/in^2, determined from mean slopes of force-indentation curves.

Material	Present investigation[a]			Crook's investigation[b]			Tabor's investigation[c]		
	p_{o_D}, dynamic	p_{o_S}, static	p_{o_D}/p_{o_S}	p_{o_D}, dynamic	p_{o_S}, static	p_{o_D}/p_{o_S}	p_{o_D}, dynamic	p_{o_S}, static	p_{o_D}/p_{o_S}
Steel, hard	986,000	952,000	1.035	.....	.....	.....	.....	.....	....
Steel, soft	588,000	485,000	1.212	.....	.....	.....	.....	.....	1.09
Aluminum	175,000	165,000	1.065	362,000	333,000	1.085	.....	.....	1.10
Lead	6,650	5,200	1.275	8,690	6,950	1.250	8,670	7,820	1.11

[a] $\frac{1}{2}$-in.-diameter steel ball striking plane-ended rods; maximum velocity = 300 ft/sec.

[b] $\frac{1}{4}$-in.-diameter steel ball bearing striking flat specimens; maximum velocity = 2 ft/sec (Ref. 71).

[c] 5-cm-diameter ball dropped from a height of 300 cm onto a massive anvil (Ref. 66).

300%, for a cone angle $2\beta = 60$ degrees, than for the spherical projectile. The ratio of these mean peak pressures for the two types of projectile geometry appeared to vary linearly with the lowest hardness number of the two bodies involved in the collision.

The results presented in Fig. 25 and 26 (Ref. 76) were obtained in an attempt to more clearly define the transition of the force-indentation relations between spherical and conical strikers. While again no distinct separation in the characteristic shape of the curves could be observed and a simple functional relation for these graphs could not be determined, the blunter strikers--as measured by an increase of the radius of the hemispherical tip--produced a greater maximum contact force and a smaller maximum and permanent indentation. The variation of the curves with tip radius at constant cone angle is very similar to that shown in Fig. 24 representing changes in the cone angle; both sets of data reveal the tremendous influence of the bluntness, or "aspect ratio" of the striker on penetration efficiency.

An analysis of the restitution processes in terms of a power law between the force of contact and the crater recovery, $\alpha - \alpha_r$, did not yield any conclusive results since minute changes in the calculated value of the permanent indentation, α_r, produced significant variations in the value of the exponent. For all types of strikers, the exponent of the recovery relation

$$F = k(\alpha-\alpha_r)^n \qquad (51)$$

ranged from 1–3, depending upon the materials and hardness of the bodies involved and on the initial velocity.

The duration of contact and dimensions of the permanent crater measured for the impact of $\frac{1}{2}$-inch-diameter spheres on $\frac{1}{2}$-inch square rods virtually coincided with results obtained for the transverse impact on bars of the same cross section at identical initial velocities (Ref. 78 and 79), indicating that the peak forces produced under these circumstances should be comparable. This is substantiated by a computation of the peak force produced by such a $\frac{1}{2}$-inch-diameter steel sphere striking a simply supported $\frac{1}{2}$- by $\frac{1}{2}$- by 24-inch mild steel beam at an impact velocity of 150 ft/sec by means of Eq. 28, which yields a maximum force of 9,300 pounds compared to a value of about 8,000 pounds obtained by interpolation of Fig. 3.

The determination of experimental force-indentation curves for large-sized projectiles becomes difficult, and it would be desirable to develop a procedure for extrapolating the experimental relations outside the range of the present tests. Furthermore, it is necessary to check the validity of the data presented by comparing experimental results obtained for the collision of strikers with other systems with corresponding calculated values, using the indentation relations previously derived in

conjunction with the deformation of such systems under a time-dependent load. In order to achieve these objectives, a dynamic force-indentation relation for the impact of a 1-inch-diameter hard steel sphere striking a mild steel target was constructed both by a combination of Eq. 41 and Fig. 16, and by increasing the statically determined relation by the factor of 50% indicated as the ratio of static to dynamic properties for this material. The outcome of this procedure is shown in Fig. 27; the restitution paths have been interpolated both from the static tests and from the dynamic data obtained with ½-inch-diameter spheres. It may be noted that the two schemes for ascertaining the dynamic force-indentation relation for this case are in reasonably close correspondence. The history of the central deflection of a ¼- by 2- by 24-inch mild steel beam supported on 30 lb/in springs at the ends under the action of a central transverse impact by a hard steel sphere of 1-inch diameter at a velocity of 28.8 ft/sec was now computed with the aid of Fig. 27 and a procedure previously developed (Ref. 83) in accordance with the equation

$$w(\tfrac{1}{2}L,t)=\frac{1}{\rho A}\sum_{i=1}^{\infty}\frac{\left[X_i(\frac{L}{2})\right]^2}{\omega_i\int_o^L X_i^2\,dx}\int_o^t F(\tau)\sin\omega_i(t-\tau)d\tau = v_o t-\frac{1}{m}\int_o^t dt\int_o^t F dt-\alpha \tag{52}$$

The time variation of the outer fiber stress determined from these calculations by means of the equation

$$\sigma = -Eb\frac{\partial^2 w}{\partial x^2} \tag{53}$$

where b is the half-beam depth, are compared to corresponding experimental data in Fig. 28 (Ref. 83). The same computation performed on the basis of the Hertz law, Eq. 39, is also presented; it may be noted that the test results are about equally well described on the basis of either type of force-indentation relation. The use of the plastic indentation relation is to be preferred, however, since the latter correctly predicts the size of the permanent crater, which cannot be deduced from the elastic law governing the formation of the dent. The highly satisfactory agreement between analysis and experimental results for this example also lends a considerable measure of confidence to the application of the experimental force-indentation curves to other collision conditions.

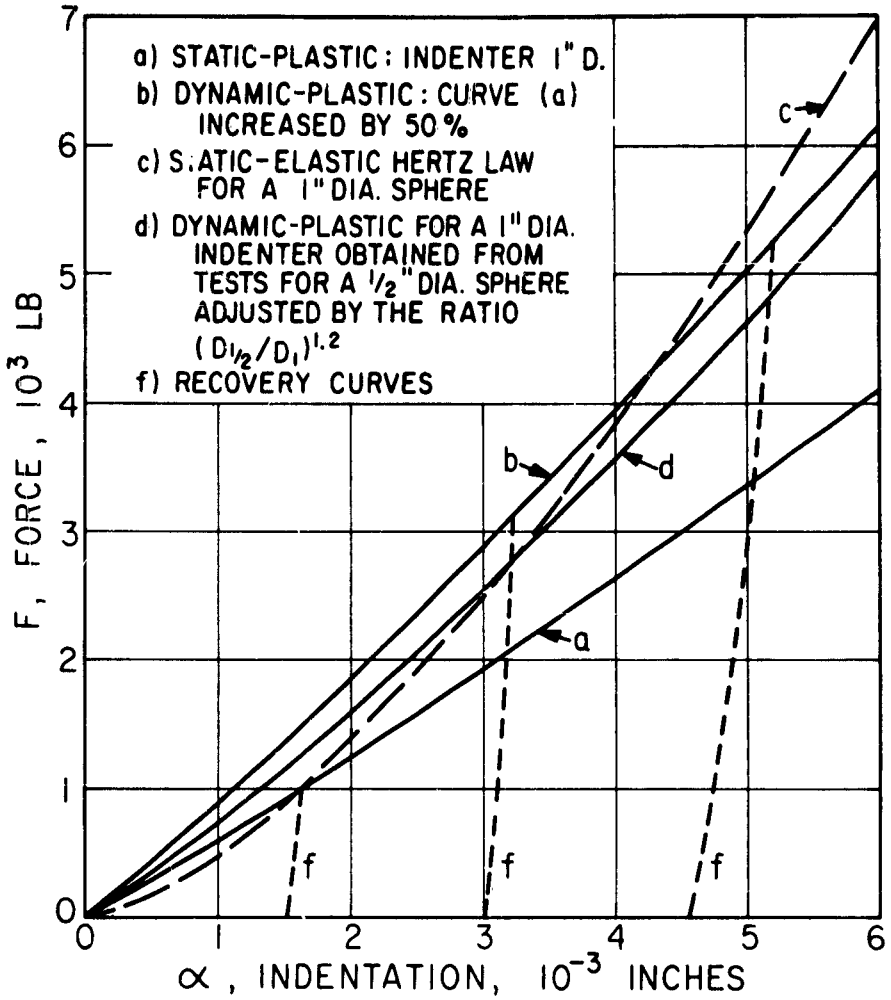

FIG. 27. Elastic and Plastic Force-Indentation Curves Under Static and Dynamic Conditions Deduced From Theory and Experimental Results for a 1-Inch-Diameter Hard Steel Sphere Penetrating a Plane Surface of Cold-Rolled Mild Steel.

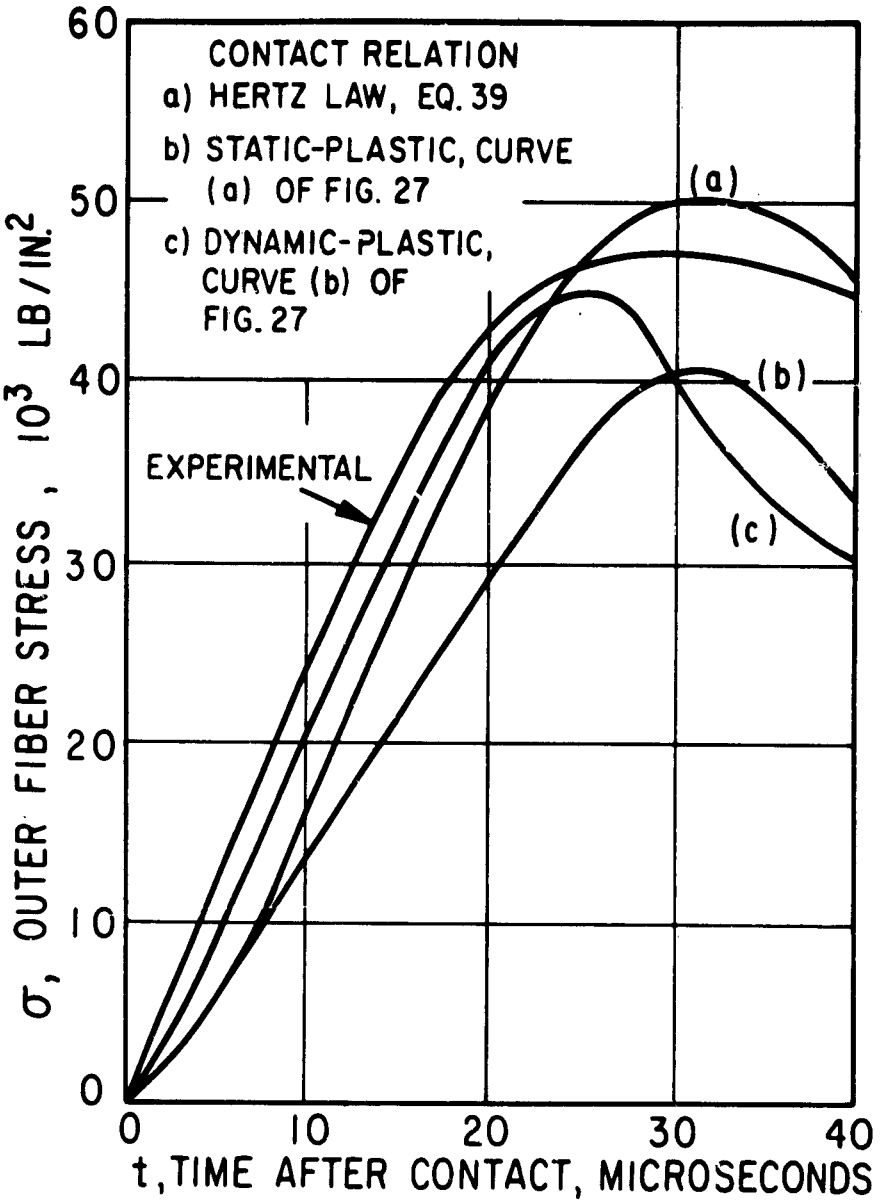

FIG. 28. Experimental and Theoretical Stress-Time Histories at the Outer Fiber of the Center of a $\frac{1}{4}$- by 2- by 24-Inch Cold-Rolled Mild Steel Beam Supported at the Ends on 30-lb/in Springs When Subjected to Central Transverse Impact by a 1-Inch-Diameter Hard Steel Sphere at a Velocity of 28.8 ft/sec.

REFERENCES

1. Davies, R. M. "The Determination of Static and Dynamic Yield Stresses Using a Steel Ball," ROY SOC LONDON, PROC, A, Vol. 197 (1949), p. 416.

2. Rayleigh, J. W. S. "On the Production of Vibrations by Forces of Relatively Long Duration, with Applications to the Theory of Collisions," PHIL MAG, Ser. 6, Vol. 11 (1906), p. 283.

3. Miklowitz, J. "Recent Developments in Elastic Wave Propagation," APPL MECH REV, Vol. 13, No. 12 (December 1960), p. 1.

4. Kolsky, H. Stress Waves in Solids. Oxford, Clarendon, 1953.

5. Abramson, H. N., H. J. Plass, and E. A. Ripperger. "Stress Wave Propagation in Rods and Beams," in Advances in Applied Mechanics. New York, Academic, 1958. Vol. 5, p. 111.

6. Davies, R. M. "Stress Waves in Solids," in Surveys in Mechanics. Cambridge, University Press, 1956. P. 64.

7. Ewing, W. M., W. S. Jardetsky, and F. Press. Elastic Waves in Layered Media. New York, McGraw-Hill, 1957.

8. Davies, R. M. "Stress Waves in Solids," APPL MECH REV, Vol. 6, No. 1 (January 1953), p. 1.

9. Cristescu, N. Probleme Dinamice in Teoria Plasticităţii. Bucuresti, Academia Republicii Populare Romîne, Ştiinţă şi Technică, No. 13, 1958.

10. Kolsky, H. "Experimental Wave-Propagation in Solids," Structural Mechanics, Proceedings of the First Symposium on Naval Structural Mechanics. New York, Pergamon, 1960. P. 233.

11. Broberg, K. B. Shock Waves in Elastic and Elastic-Plastic Media. Stockholm, Avhandling Kungl. Tekniska Högskolan, No. 111, 1956.

12. Hopkins, H. G. "Dynamic Anelastic Deformations of Metals," APPL MECH REV, Vol. 14, No. 6 (June 1961), p. 1.

13. Goldsmith, W. Impact. London, Edward Arnold, 1960.

14. Love, A. E. H. A Treatise on the Mathematical Theory of Elasticity. New York, Dover, 1944.

15. Davies, R. M. "A Critical Study of the Hopkinson Pressure Bar," RCY SOC LONDON, PHIL TRANS, A, Vol. 240 (1948), p. 375.

16. Rayleigh, J. W. S. "On Waves Propagated Along the Plane Surface of an Elastic Solid," LONDON MATH SOC, PROC, Vol. 17 (1885), p. 4.

17. ------. "On the Free Vibrations of an Infinite Plate of Homogeneous, Isotropic Elastic Matter," LONDON MATH SOC, PROC, Vol. 20 (1889), p. 225.

18. Lamb, H. "On Waves in an Elastic Plate," ROY SOC LONDON, PROC, A, Vol. 93 (1917), p. 114.

19. Pochhammer, L. "Über die Fortpflanzungsgeschwindigkeiten kleiner Schwingungen in einem unbegrenzten isotropen Kreiszylinder," J REINE ANGEW MATH (Crelle), Vol. 81 (1876), p. 324.

20. Chree, C. "The Equations of an Isotropic Elastic Solid in Polar and Cylindrical Coordinates, Their Solution and Application," CAMBRIDGE PHIL SOC, TRANS, Vol. 14 (1889), p. 250.

21. Abramson, H. N. "Flexural Waves in Elastic Beams of Circular Cross Section," ACOUS SOC AM, J, Vol. 29 (1957), p. 42.

22. Green, W. A. "Dispersion Relations for Elastic Waves in Bars," in Progress in Solid Mechanics. Amsterdam, North-Holland, 1960. Vol. 1, p. 225.

23. Herrmann, G., and I. Mirsky. "Three Dimensional and Shell Theory Analysis of Axially-Symmetric Motions of Cylinders," J APPL MECH, Vol. 23 (1956), p. 563.

24. Mirsky, I., and G. Herrmann. "Axially Symmetric Motions of Thick Cylindrical Shells," J APPL MECH, Vol. 25 (1958), p. 97.

25. ------. "Nonaxially Symmetric Motions of Cylindrical Shells," ACOUS SOC AM, J, Vol. 29 (1957), p. 1116; Vol. 31 (1959), p. 250.

26. Greenspon, J. E. "Flexural Vibrations of a Thick-Walled Circular Cylinder According to the Exact Theory of Elasticity," J AERO/SPACE SCI, Vol. 27 (1960), p. 37.

27. ------. "Vibrations of Thick Shells in a Vacuum," ACOUS SOC AM, J, Vol. 31 (1959), p. 1682.

28. Gazis, D. C. "Three Dimensional Investigation of the Propagation of Waves in Hollow Circular Cylinders. I. Analytical Foundation. II. Numerical Results," ACOUS SOC AM, J, Vol. 31 (1959), p. 568.

29. Kalnins, A., and P. M. Naghdi. "Propagation of Axisymmetric Waves in an Unlimited Elastic Shell," J APPL MECH (ASME, TRANS, Ser. E), Vol. 27 (1960), p. 690.

30. Sherwood, J. W. C. "Propagation in an Infinite Elastic Plate," ACOUS SOC AM, J, Vol. 30 (1958), p. 979.

31. Mindlin, R. D., and H. D. McNiven. "Axially Symmetric Waves in Elastic Rods," J APPL MECH (ASME, TRANS, Ser. E), Vol. 27 (1960), p. 145.

32. Mindlin, R. D. "Waves and Vibrations in Isotropic Elastic Plates," Structural Mechanics, Proceedings of the First Symposium on Naval Structural Mechanics. New York, Pergamon, 1960. P. 199.

33. Oliver, J. "Elastic Wave Dispersion in a Cylindrical Rod by a Wide-Band Short-Duration Pulse Technique," ACOUS SOC AM, J, Vol. 29 (1957), p. 189.

34. Curtis, C. W. "Second Mode Vibrations of the Pochhammer-Chree Frequency Equation," J APPL PHYS, Vol. 25 (1954), p. 928.

35. Devault, C. P., and C. W. Curtis. "Problem of Elastic Bar with Mixed Time-Dependent End Conditions of General Form," ACOUS SOC AM, J, Vol. 31 (1959), p. 635.

36. Ripperger, E. A., and H. N. Abramson. "A Study of the Propagation of Flexural Waves in Elastic Beams," J APPL MECH, Vol. 24 (1957), p. 431.

37. Bishop, R. E. D. "Longitudinal Waves in Beams," AERONAUT QUART, Vol. 3 (1952), p. 280.

38. Mindlin, R. D., and G. Herrmann. "A One-Dimensional Theory of Compressional Waves in an Elastic Rod," Proceedings of the First U. S. National Congress of Applied Mechanics, 1952, p. 187.

39. Miklowitz, J. "The Propagation of Compressional Waves in a Dispersive Elastic Rod. I: Results from the Theory," J APPL MECH, Vol. 24 (1957), p. 231.

40. Miklowitz, J., and C. R. Nisewanger. "The Propagation of Compressional Waves in a Dispersive Elastic Rod. II: Experimental Results and Comparison with Theory," J APPL MECH, Vol. 24 (1957), p. 240.

41. Miklowitz, J. "On the Use of Approximate Theories of an Elastic Rod in Problems of Longitudinal Impact," Proceedings of the Third U. S. National Congress of Applied Mechanics, 1958, p. 215.

42. Prescott, J. "Elastic Waves and Vibrations of Thin Rods," PHIL MAG, Ser. 7, Vol. 33 (1942), p. 703.

43. Volterra, E. "Equations of Motion for Curved Elastic Bars Deduced by Use of 'Method of Internal Constraints,'" ING-ARCH, Vol. 23 (1955), p. 410.

44. Kynch, G. J. "Fundamental Modes of Vibration of Uniform Beams for Medium Wavelengths," BRIT J APPL PHYS, Vol. 8 (1957), p. 64.

45. Boley, B. A. "An Approximate Theory of Lateral Impact on Beams," J APPL MECH, Vol. 22 (1955), p. 69.

46. Dengler, M. A., and M. Goland. "Transverse Impact on Long Beams, Including Rotatory Inertia and Shear Effects," Proceedings of the First U. S. National Congress of Applied Mechanics, 1952, p. 179.

47. Timoshenko, S. P. "On the Transverse Vibrations of Bars of Uniform Cross Section," PHIL MAG, Ser. 6, Vol. 43 (1922), p. 125.

48. Sato, Y. "Velocity of Elastic Waves Propagated in Media with Small Holes," EARTHQUAKE RES INST (Tokyo), BULL, Vol. 30 (1952), p. 1.

49. Brandt, H. "A Study of the Speed of Sound in Porous Granular Media," J APPL MECH, Vol. 22 (1955), p. 479.

50. Duffy, J., and R. D. Mindlin. "Stress-Strain Relations and Vibrations of a Granular Medium," J APPL MECH, Vol. 24 (1957), p. 585.

51. Deresiewicz, H. "Stress-Strain Relations for a Simple Model of a Granular Medium," J APPL MECH, Vol. 25 (1958), p. 402.

52. Lee, E. H., and T. Kanter. "Wave Propagation in Finite Rods of Viscoelastic Materials," J APPL PHYS, Vol. 24 (1953), p. 1115.

53. Glanz, R. D., and E. H. Lee. "Transient Wave Analysis in a Linear Time-Dependent Material," J APPL PHYS, Vol. 25 (1954), p. 947.

54. Lee, E. H., and J. A. Morrison. "A Comparison of the Propagation of Longitudinal Waves in Rods of Viscoelastic Materials," J POLYMER SCI, Vol. 19 (1956), p. 93.

55. Berry, D. S., and S. C. Hunter. "The Propagation of Dynamic Stresses in Visco-elastic Rods," J MECH PHYS SOLIDS, Vol. 4 (1956), p. 72.

56. Berry, D. S. "Stress Propagation in Visco-Elastic Bodies," J MECH PHYS SOLIDS, Vol. 6 (1958), p. 177.

57. Bland, D. R. The Theory of Linear Viscoelasticity. New York, Pergamon, 1960.

58. Hillier, K. W., and H. Kolsky. "An Investigation of the Dynamic Elastic Properties of Some High Polymers," PHYS SOC LONDON, PROC, B, Vol. 62 (1949), p. 111.

59. Kolsky, H. "The Propagation of Stress Pulses in Viscoelastic Solids," PHIL MAG, Ser. 8, Vol. 1 (1956), p. 693.

60. Hunter, S. C. "Viscoelastic Waves," in Progress in Solid Mechanics, Amsterdam, North-Holland, 1960. Vol. 1, p. 1.

61. Hertz, H. "Über die Berührung fester elastischer Körper," J REINE ANGEW MATH (Crelle), Vol. 92 (1881), p. 155.

62. Pao, Y.-P. "Extension of the Hertz Theory of Impact to the Visco-elastic Case," J APPL PHYS, Vol. 26 (1955), p. 1083.

63. Hunter, S. C. "The Hertz Problem for a Rigid Spherical Indenter and a Viscoelastic Half-Space," J MECH PHYS SOLIDS, Vol. 8 (1960), p. 219.

64. Lee, E. H., and J. R. M. Radok. "Contact Problem for Viscoelastic Bodies," J APPL MECH (ASME, TRANS, Ser. E), Vol. 27 (1960), p. 438.

65. Meyer, E. "Untersuchungen über Härteprüfung und Härte," VEREIN DEUT ING ZEITS, Vol. 42 (1908), p. 645.

66. Tabor, D. The Hardness of Metals. Oxford, Clarendon, 1951.

67. Berger, F. Das Gesetz des Kraftverlaufes beim Stoss. Braunschweig, F. Vieweg and Sohn, 1924.

68. Pöschl, T. Der Stoss. Handbuch der Physik. Berlin, J. Springer, 1926. Vol. 6, Chap. 7.

69. Andrews, J. P. "Experiments on Impact," PHYS SOC LONDON, PROC, Vol. 43 (1931), p. 8.

70. ------. "Theory of Collision of Spheres of Soft Metal," PHIL MAG, Ser. 7, Vol. 9 (1930), p. 593.

71. Crook, A. W. "A Study of Some Impacts Between Metal Bodies by a Piezoelectric Method," ROY SOC LONDON, PROC, A, Vol. 212 (1952), p. 377.

72. Davis, C. D., and S. C. Hunter. "Assessment of the Strain-Rate Sensitivity of Metals by Indentation with Conical Indenters," J MECH PHYS SOLIDS, Vol. 8 (1960), p. 235.

73. Nishiwaki, J. "Resistance to the Penetration of a Bullet Through an Aluminum Plate," PHYS SOC JAPAN, J, Vol. 6 (1951), p. 374.

74. Goldsmith, W., and P. T. Lyman. "The Penetration of Hard-Steel Spheres into Plane Metal Surfaces," J APPL MECH (ASME, TRANS, Ser. E), Vol. 27 (1960), p. 717.

75. Goldsmith, W., and C.-H. Yew. "Penetration of Conical Indenters into Plane Metal Surfaces," Proceedings of the Fourth U. S. National Congress of Applied Mechanics, 1962. Vol. 1, p. 177.

76. Tang, W. "The Penetration of Conical Indenters with Hemispherical Tips into Plane Metal Surfaces," Thesis (M.S.), Univ. of California, Berkeley, 1962.

77. Ripperger, E. A. "The Propagation of Pulses in Cylindrical Bars--An Experimental Study," Proceedings of the First Midwestern Conference on Solid Mechanics, 1953, p. 29.

78. Cunningham, D. M., and W. Goldsmith. "Short-Time Impulses Produced by Longitudinal Impact," SOC EXPL STRESS ANAL, PROC, Vol. 16, No. 2 (1959), p. 153.

79. Goldsmith, W., and D. M. Cunningham. "Kinetics of Oblique Impact of a Sphere on a Beam," J APPL MECH, Vol. 23 (1956), p. 612.

80. Baker, W. E., and R. C. Dove. "Measurement of Internal Strains in a Bar Subjected to Longitudinal Impact," EXPL MECH, Vol. 2, No. 10 (1962), p. 307.

81. Sears, J. E. "On the Longitudinal Impact of Metal Rods with Rounded Ends," CAMBRIDGE PHIL SOC, TRANS, Vol. 21 (1908), p. 49.

82. Whiffin, A. C. "The Use of Flat-Ended Projectiles for Determining Dynamic Yield Stress. II: Tests on Various Metallic Materials," ROY SOC LONDON, PROC, A, Vol. 194 (1948), p. 300.

83. Barnhart, K. E., Jr., and W. Goldsmith. "Transverse Impact on Elastically Supported Beams," J APPL MECH, Vol. 24 (1957), p. 440.

ACKNOWLEDGMENT

The author is indebted to Professor D. M. Cunningham and Messrs. P. T. Lyman, Jr. and W. Tang of the University of California, Berkeley, Professor C.-H. Yew of the University of Texas, and Dr. K. E. Barnhart of Fresno State College.

INITIAL DISTRIBUTION

19 Chief, Bureau of Naval Weapons
- DLI-31 (2)
- RAAV (1)
- RAAV-34 (1)
- RM-3 (1)
- RMMO-4 (2)
- RMMO-5 (1)
- RMMO-512 (1)
- RMMO-522 (1)
- RR (1)
- RRRE (1)
- RRRE-5 (1)
- RSSH-32 (1)
- RU (1)
- RUME-11 (1)
- RUME-3 (2)
- RUTO-2 (1)

5 Chief of Naval Operations
- Deputy Chief for Air (1)
- Operations Evaluation Group (2)
- OP-55 (1)
- OP-721D (1)

3 Chief of Naval Research
- Code 104 (1)
- Code 429 (1)
- Code 461 (1)

1 Air Development Squadron 5, Naval Air Facility, China Lake
1 David W. Taylor Model Basin
1 Fleet Anti-Air Warfare Training Center, San Diego
1 Naval Air Force, Atlantic Fleet
2 Naval Air Force, Pacific Fleet
1 Naval Air Material Center, Philadelphia
2 Naval Air Mobile Training, Naval Air Station, Miramar
- Naval Air Mobile Training Detachment, 4003 Ordnance (1)
- Naval Air Mobile Training Detachment, 4030 Missile (1)

1 Naval Air Station, North Island
2 Naval Air Test Center, Patuxent River (Aeronautical Publications Library)
1 Naval Avionics Facility, Indianapolis (Library)
1 Naval Explosive Ordnance Disposal Facility, Naval Propellant Plant, Indian Head
1 Naval Missile Center, Point Mugu (Technical Library)

ABSTRACT CARD

U. S. Naval Ordnance Test Station
Impact at Intermediate Velocities Involving Contact Phenomena, by Werner Goldsmith. China Lake, Calif., NOTS, March 1963. 58 pp. (NAVWEPS Report 8088, NOTS TP 3125), UNCLASSIFIED.

(Over)
2 cards, 4 copies

U. S. Naval Ordnance Test Station
Impact at Intermediate Velocities Involving Contact Phenomena, by Werner Goldsmith. China Lake, Calif., NOTS, March 1963. 58 pp. (NAVWEPS Report 8088, NOTS TP 3125), UNCLASSIFIED.

(Over)
2 cards, 4 copies

U. S. Naval Ordnance Test Station
Impact at Intermediate Velocities Involving Contact Phenomena, by Werner Goldsmith. China Lake, Calif., NOTS, March 1963. 58 pp. (NAVWEPS Report 8088, NOTS TP 3125), UNCLASSIFIED.

(Over)
2 cards, 4 copies

U. S. Naval Ordnance Test Station
Impact at Intermediate Velocities Involving Contact Phenomena, by Werner Goldsmith. China Lake, Calif., NOTS, March 1963. 58 pp. (NAVWEPS Report 8088, NOTS TP 3125), UNCLASSIFIED.

(Over)
2 cards, 4 copies

NAVWEPS Report 8088

ABSTRACT. Theoretical relations and experimental data are presented for the collision of two objects at intermediate velocities when both wave propagation and relative indentation of the bodies must be considered. Equations are developed that combine a description of wave phenomena in beams, bars, and plates with a law of contact. Experimental results are shown involving the impact of spheres and conically headed projectiles on bars and beams, and a comparison with the predictions of several theories is provided.

The analytical relations are based on equations

(Contd. on Card 2)

NAVWEPS Report 8088

ABSTRACT. Theoretical relations and experimental data are presented for the collision of two objects at intermediate velocities when both wave propagation and relative indentation of the bodies must be considered. Equations are developed that combine a description of wave phenomena in beams, bars, and plates with a law of contact. Experimental results are shown involving the impact of spheres and conically headed projectiles on bars and beams, and a comparison with the predictions of several theories is provided.

The analytical relations are based on equations

(Contd. on Card 2)

NAVWEPS Report 8088

ABSTRACT. Theoretical relations and experimental data are presented for the collision of two objects at intermediate velocities when both wave propagation and relative indentation of the bodies must be considered. Equations are developed that combine a description of wave phenomena in beams, bars, and plates with a law of contact. Experimental results are shown involving the impact of spheres and conically headed projectiles on bars and beams, and a comparison with the predictions of several theories is provided.

The analytical relations are based on equations

(Contd. on Card 2)

NAVWEPS Report 8088

ABSTRACT. Theoretical relations and experimental data are presented for the collision of two objects at intermediate velocities when both wave propagation and relative indentation of the bodies must be considered. Equations are developed that combine a description of wave phenomena in beams, bars, and plates with a law of contact. Experimental results are shown involving the impact of spheres and conically headed projectiles on bars and beams, and a comparison with the predictions of several theories is provided.

The analytical relations are based on equations

(Contd. on Card 2)

ABSTRACT CARD

U. S. Naval Ordnance Test Station
Impact at Intermediate . . . (Card 2)
of motion treating both bars and beams as one-dimensional systems, with the effect of second-order correction factors neglected. The theory of Hertz and a simple postulate concerning perfectly plastic flow at the contact point are compared with the results of tests designed to relate experimentally the contact force as a function of the indentation in a regime where the major portion of the cross

(Over)
NAVWEPS Report 8088

U. S. Naval Ordnance Test Station
Impact at Intermediate . . . (Card 2)
of motion treating both bars and beams as one-dimensional systems, with the effect of second-order correction factors neglected. The theory of Hertz and a simple postulate concerning perfectly plastic flow at the contact point are compared with the results of tests designed to relate experimentally the contact force as a function of the indentation in a regime where the major portion of the cross

(Over)
NAVWEPS Report 8088

U. S. Naval Ordnance Test Station
Impact at Intermediate . . . (Card 2)
of motion treating both bars and beams as one-dimensional systems, with the effect of second-order correction factors neglected. The theory of Hertz and a simple postulate concerning perfectly plastic flow at the contact point are compared with the results of tests designed to relate experimentally the contact force as a function of the indentation in a regime where the major portion of the cross

(Over)
NAVWEPS Report 8088

U. S. Naval Ordnance Test Station
Impact at Intermediate . . . (Card 2)
of motion treating both bars and beams as one-dimensional systems, with the effect of second-order correction factors neglected. The theory of Hertz and a simple postulate concerning perfectly plastic flow at the contact point are compared with the results of tests designed to relate experimentally the contact force as a function of the indentation in a regime where the major portion of the cross

(Over)
NAVWEPS Report 8088

section at the point of contact remains elastic. The data were obtained from strain-gage and framing camera measurements.

NAVWEPS Report 8088

section at the point of contact remains elastic. The data were obtained from strain-gage and framing camera measurements.

NAVWEPS Report 8088

section at the point of contact remains elastic. The data were obtained from strain-gage and framing camera measurements.

NAVWEPS Report 8088

section at the point of contact remains elastic. The data were obtained from strain-gage and framing camera measurements.